Available online at www.sciencedirect.com
ScienceDirect
Journal of the Mechanics and Physics of Solids 56 (2008) 25–50
JOURNAL OF THE MECHANICS AND PHYSICS OF SOLIDS
www.elsevier.com/locate/jmps

Transition of mode II cracks from sub-Rayleigh to intersonic speeds in the presence of favorable heterogeneity

Yi Liu[a], Nadia Lapusta[b,*]

[a]*Division of Engineering and Applied Science, California Institute of Technology, Pasadena, CA 91125, USA*
[b]*Division of Engineering and Applied Science and Division of Geological and Planetary Sciences, California Institute of Technology, Pasadena, CA 91125, USA*

Received 22 January 2007; received in revised form 8 June 2007; accepted 11 June 2007

Abstract

Understanding sub-Rayleigh-to-intersonic transition of mode II cracks is a fundamental problem in fracture mechanics with important practical implications for earthquake dynamics and seismic radiation. In the Burridge–Andrews mechanism, an intersonic daughter crack nucleates, for sufficiently high prestress, at the shear stress peak traveling with the shear wave speed in front of the main crack. We find that sub-Rayleigh-to-intersonic transition and sustained intersonic propagation occurs in a number of other models that subject developing cracks to intersonic loading fields. We consider a spontaneously expanding sub-Rayleigh crack (or main crack) which advances, along a planar interface with linear slip-weakening friction, towards a place of favorable heterogeneity, such as a preexisting subcritical crack or a small patch of higher prestress (similar behavior is expected for a small patch of lower static strength). For a range of model parameters, a secondary dynamic crack nucleates at the heterogeneity and acquires intersonic speeds due to the intersonic stress field propagating in front of the main crack. Transition to intersonic speeds occurs directly at the tip of the secondary crack, with the tip accelerating rapidly to values numerically equal to the Rayleigh wave speed and then abruptly jumping to an intersonic speed. Models with favorable heterogeneity achieve intersonic transition and propagation for much lower prestress levels than the ones implied by the Burridge–Andrews mechanism and have transition distances that depend on the position of heterogeneity. We investigate the dependence of intersonic transition and subsequent crack propagation on model parameters and discuss implications for earthquake dynamics.

Keywords: Dynamic fracture; Supershear transition of earthquakes; Crack mechanics; Elastic material; Boundary integral equations

1. Introduction

Understanding sub-Rayleigh-to-intersonic transition of mode II cracks is a fundamental problem in fracture mechanics with important practical implications for earthquake dynamics and seismic radiation. In this work, the word "intersonic" refers to speeds between the shear wave speed c_s and the dilatational wave speed c_p, the range which is often called "supershear" in the geophysical literature. Large strike-slip

*Corresponding author. Tel.: +1 626 395 2277; fax: +1 626 583 4963.
E-mail address: lapusta@caltech.edu (N. Lapusta).

0022-5096/$ - see front matter © 2007 Elsevier Ltd. All rights reserved.
doi:10.1016/j.jmps.2007.06.005

earthquakes are dominated by in-plane sliding and some of their dynamics can be understood by considering them as mode II cracks. Although average rupture speeds for earthquakes are sub-Rayleigh in general, seismic data for several earthquakes points to intersonic propagation. Examples are 1979 Imperial Valley earthquake (Archuleta, 1984; Spudich and Cranswick, 1984), 1992 Landers earthquake (Olsen et al., 1997), 1999 Izmit earthquake (Bouchon et al., 2001), 2001 Kunlun earthquake (Bouchon and Vallée, 2003), and 2002 Denali earthquake (Ellsworth et al., 2004). While this evidence is indirect, as it is obtained through analysis of seismic data, it presents a compelling case that intersonic propagation and hence sub-Rayleigh-to-intersonic rupture transition may occur during earthquakes.

Direct evidence for the possibility of spontaneous intersonic transition and propagation has been obtained in the laboratory. Intersonic crack propagation of mode II cracks was observed on weak interfaces under impact loading conditions (Rosakis et al., 1999; Rosakis, 2002). Needleman and Rosakis (1999) numerically modeled those experiments and qualitatively reproduced their crack speed histories. Xia et al. (2004) reported experimental observations of spontaneous sub-Rayleigh-to-intersonic transition of mode II cracks propagating along a frictionally held homogeneous interface. Xia et al. (2005) experimentally observed a change in rupture speed from sub-Rayleigh to intersonic along a bi-material interface.

Studies of sub-Rayleigh-to-intersonic transition have important practical implications. On the one hand, understanding which parameters and conditions do, and do not, lead to intersonic rupture propagation in models can help constrain properties and stress conditions on those faults where rupture speeds of large earthquakes have been inferred. On the other hand, it is important to know which conditions can lead to intersonic propagation on faults and how likely are intersonic ruptures to occur. This is because intersonic ruptures can cause much stronger shaking far from the fault than subsonic ruptures can, as Mach fronts generated by intersonic ruptures carry large stresses and particle velocities far from the fault (Bernard and Baumont, 2005; Dunham and Archuleta, 2005; Bhat et al., 2007).

Theoretical and numerical studies of sub-Rayleigh-to-intersonic transition date back to Burridge (1973) and Andrews (1976). Burridge (1973) considered a self-similar mode II crack and found that a shear stress peak propagates with the shear wave speed c_s in front of the crack. Andrews (1976) performed numerical simulations of spontaneous crack propagation on a uniformly prestressed interface governed by a linear slip-weakening law (Fig. 1a) in which friction linearly decreases from static friction strength τ^s to constant dynamic friction strength τ^d over a characteristic slip d_0. This law implies a finite fracture energy given by $\frac{1}{2}(\tau^s-\tau^d)d_0$. Andrews (1976) started with shear stress and slip distributions appropriate for a critical static crack under a uniform far-field shear loading τ^o and initiated a dynamic crack by slightly increasing shear stress along the critical crack profile. The half length of the critical crack is given by (Andrews, 1976):

$$L^c = \frac{1}{\pi(1-\nu)}\frac{\mu(\tau^s-\tau^d)d_0}{(\tau^o-\tau^d)^2}, \tag{1}$$

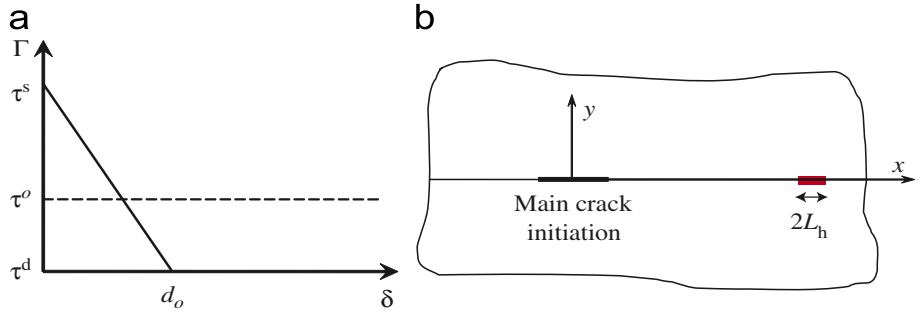

Fig. 1. (a) Linear slip-weakening friction law. Γ is the shear strength of the interface and δ is slip (or relative displacement in shear) across the interface. (b) A prescribed crack interface is embedded in an infinite, elastic, and homogeneous space. The main crack is initiated from a region around $x=0$. This work considers interaction of the main crack with a region of heterogeneity that exists in front of the main crack and may initiate a secondary crack. Depending on the model, the heterogeneity is a preexisting subcritical crack, a patch with higher prestress, or a patch with lower static friction strength. When discussing crack tips and their speeds for both main and secondary cracks, we always refer to crack tips that propagate in the direction of increasing x, or to the right in all figures, unless specified otherwise.

where ν is the Poisson's ratio and μ is the shear modulus. L^c is used as a reference length scale in this study, to facilitate comparison with Andrews (1976) and subsequent studies. Andrews (1976) confirmed and supplemented the findings of Burridge (1973) by demonstrating that a growing shear stress peak propagates with the shear wave speed c_s in front of the initially sub-Rayleigh crack and that the peak approaches the limiting value $\tau^{max} = \tau^o + S_{crit}(\tau^o - \tau^d)$, $S_{crit} = 1.77$, as the crack approaches the Rayleigh wave speed c_R. If $\tau^{max} > \tau^s$, the shear stress peak reaches static friction strength during crack propagation, and a daughter crack is initiated in front of the main crack. The daughter crack propagates with intersonic speeds from its very beginning. This process of intersonic transition is often called the Burridge–Andrews mechanism. Fig. 2 shows our simulation of this transition mechanism; the methodology is described in Section 2.

The Burridge–Andrews mechanism has been observed in the laboratory (Xia et al., 2004) and provides a plausible model for intersonic transition during earthquakes. The condition $\tau^{max} > \tau^s$ implies that, for given friction properties, shear prestress τ^o on the interface has to be large enough for intersonic transition to occur, i.e., $(\tau^o - \tau^d)/(\tau^s - \tau^d) > 1/(1 + S_{crit}) = 0.36$. Equivalently, the seismic ratio S defined as $S = (\tau^s - \tau^o)/(\tau^o - \tau^d)$ has to be smaller than the critical value, $S_{crit} = 1.77$. If, for given friction properties, shear prestress τ^o is not large enough, no daughter crack nucleates, and the limiting rupture speed of the main crack is the Rayleigh wave speed c_R. Note that values of τ^o only slightly larger than the limiting value would imply transition to intersonic speeds at very large propagation distances, and larger values of τ^o are needed for smaller transition distances. For example, transition at the location $x/L^c = 13.5$ requires prestress $(\tau^o - \tau^d)/(\tau^s - \tau^d) = 0.53$, which is the case shown in Fig. 2.

Since the pioneering work of Burridge (1973) and Andrews (1976), a number of theoretical and numerical studies have addressed the issue of sub-Rayleigh-to-intersonic transition and/or intersonic propagation. Significant advances have been made in understanding various theoretical aspects of crack propagation with speeds larger than c_R (e.g., Burridge et al., 1979; Freund, 1979; Broberg, 1994, 1995; Huang and Gao, 2001; Samudrala et al., 2002; Antipov and Willis, 2003). In part, it has been established that cracks cannot propagate with speeds in the interval $[c_R, c_s]$ due to energetic constraints, and that intersonic cracks in models with finite tractions, constant fracture energy, and uniform prestress would tend to accelerate to the dilatational wave speed c_p. Gao et al. (2001) studied the transition of a sub-Rayleigh mode II crack to intersonic speeds using both continuum and molecular dynamics simulations and showed that the two approaches agree. Geubelle and Kubair (2001) analyzed numerically intersonic transition under mixed-mode conditions and pointed out that transition from sub-Rayleigh to intersonic speeds can occur "through a sudden acceleration of the tip of the main cohesive zone". The study of Geubelle and Kubair (2001)

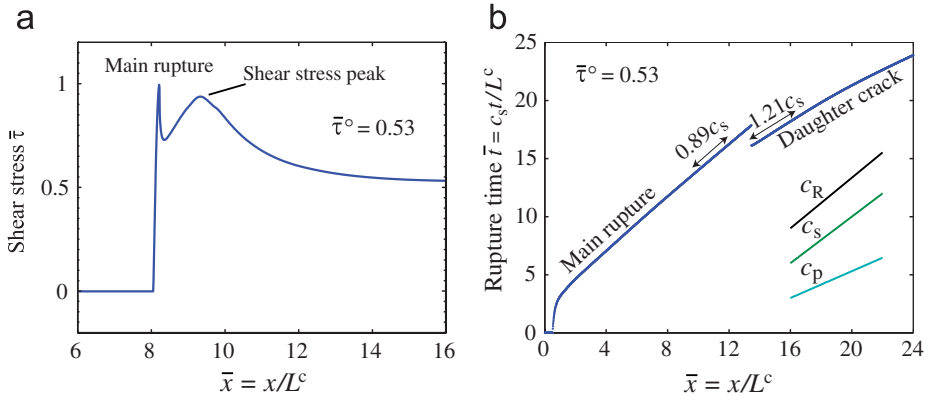

Fig. 2. (a) Shear stress distribution for a mode II crack spontaneously propagating on an interface governed by linear slip-weakening friction. A peak in shear stress travels with the shear wave speed in front of the crack. The interface has uniform friction properties and uniform prestress τ^o given by $(\tau^o - \tau^d)/(\tau^s - \tau^d) = 0.53$. (b) Rupture time along the interface, i.e., the time at which each point along the interface first acquires non-zero speeds. A daughter crack appears in front of the main crack at the location $x/L^c = 13.5$ and propagates with intersonic speeds as described by the Burridge–Andrews mechanism. Here and in the text the word "intersonic" refers to speeds between the shear wave speed c_s and the dilatational wave speed c_p. For lower prestress, the daughter crack would appear further along the interface or not at all.

considered relatively high prestress levels that would result in intersonic transition by the Burridge–Andrews mechanism. It is likely that transition in their model is influenced by the crack initiation procedure as discussed in Section 5.4. Recently, Festa and Vilotte (2006) and Shi et al. (2007) considered dependence of intersonic transition and rupture mode on crack initiation; the former study used linear slip-weakening friction, while the latter study used a law of a rate and state type. The importance of crack initiation is further discussed in Section 5.4. Dunham (2006) proposed that transition distances for the Burridge–Andrews mechanism can be obtained from the self-similar crack model by requiring that the daughter crack reaches a critical size. The idea that an intersonic crack needs to reach a critical size before it can achieve sustained intersonic propagation may help explain some of our results as discussed in Section 5.1. Intersonic transition in 3D models of earthquake rupture, in some cases in the presence of heterogeneities, have been studied numerically by a number of researchers (e.g., Day, 1982a,b; Madariaga and Olsen, 2000; Fukuyama and Olsen, 2002; Dunham et al., 2003). In particular, the 3D model of Fukuyama and Olsen (2002) included an asperity of higher prestress, as we consider in one of the models in this study. Differences between 2D and 3D models are discussed in Section 5.6. A number of studies addressed the issue of intersonic rupture speeds in a bi-material configuration, where the interface separates two different elastic materials (e.g., Harris and Day, 1997; Cochard and Rice, 2000; Adams, 2001; Ranjith and Rice, 2001; Shi and Ben-Zion, 2006).

In this work, we take a broader look at the Burridge–Andrews mechanism and find, through numerical simulations of spontaneous crack propagation, that sub-Rayleigh-to-intersonic transition occurs in a number of models where a crack is subjected to an intersonic loading stress field. The Burridge–Andrews mechanism falls under that category, as a daughter crack initiates at the location of the shear stress peak and finds itself under the influence of the stress field of the advancing main crack. That stress field creates intersonic loading in front of the shear stress peak (Appendix A). We consider interaction of an advancing mode II crack (main crack) with a location susceptible to nucleation of a secondary dynamic crack (Fig. 1b), such as a preexisting subcritical crack, a patch of higher prestress, or a patch of lower static strength. Such locations are called collectively by "favorable heterogeneity" in this work. For a range of parameters, a secondary dynamic crack initiates at the location before the shear stress peak arrives, acquires intersonic speeds, and maintains intersonic propagation for large distances. We call the crack secondary to reserve the term "daughter" for cracks that initiate at the location of the shear stress peak in front of the main crack in the absence of preexisting heterogeneity. Our results show, in part, that nucleating a daughter crack at the shear wave peak, a feature that propagates with the shear wave speed, is not essential for the subsequent intersonic propagation of the daughter crack.

The main findings of this study are: (1) Crack tips can abruptly jump from speeds approaching the Rayleigh wave speed c_R to an intersonic speed c_{sp}, $c_s < c_{sp} < c_p$. This is different from the Burridge–Andrews mechanism, in which the daughter crack is intersonic from its very beginning. (2) Intersonic rupture transition can be achieved and subsequent intersonic crack propagation can be maintained under background prestress levels that are lower than the ones predicted by the Burridge–Andrews mechanism. (3) Transition lengths depend, in our models, on the position of favorable heterogeneities, as the secondary crack acquires sustained intersonic speeds close to that position. (The intersonic transition length is defined here as the distance between the location of the main crack initiation and the location of intersonic transition.) Observations of transition lengths in earthquakes are sometimes interpreted using the Burridge–Andrews mechanism to infer parameters of fault friction (e.g., Xia et al., 2004). If intersonic transition is governed by presence of heterogeneities as considered in this work, such inferences may be misleading. These and other findings and their implications are further discussed in Section 5.

2. Methodology

We consider a mode II plane-strain shear crack propagating along a planar interface $y = 0$ embedded in an infinite, linear elastic, and homogeneous space (Fig. 1). The direction of crack propagation and slip (or relative displacement in shear) $\delta(x, t)$ is denoted by x. The Poisson's ratio ν is chosen to be 0.25, so that $c_R = 0.92c_s$ and $c_p = \sqrt{3}c_s$. The crack interface is governed by a linear slip-weakening friction law, in which its shear strength Γ linearly decreases from its static value τ^s to its dynamic value τ^d over

a characteristic slip d_0:

$$\Gamma(\delta) = \begin{cases} \tau^{\mathrm{d}} + (\tau^{\mathrm{s}} - \tau^{\mathrm{d}})(1 - \delta/d_0), & \delta \leqslant d_0, \\ \tau^{\mathrm{d}}, & \delta > d_0. \end{cases} \tag{2}$$

τ^{s} and τ^{d} can be thought of as products of constant in time compressive normal stress $\sigma(x)$ and static and dynamic friction coefficients, respectively. τ^{s} and τ^{d} are uniform in space for cases described in this study. Section 5 contains a comment about models with a patch of lower static friction strength τ^{s}.

Rupture propagation is numerically calculated using the spectral boundary integral method (e.g., Perrin et al., 1995; Geubelle and Rice, 1995; Lapusta et al., 2000). The main idea of the method is to confine the numerical consideration to the interface plane, by expressing the elastodynamic response of the surrounding elastic media in terms of integral relationships between slip and traction on the interface. In our 2D model, shear traction $\tau(x,t)$ on the interface $y=0$ can be expressed as the sum of "loading" traction $\tau^{\mathrm{l}}(x,t)$ that would act on the interface in the absence of any displacement discontinuity (i.e., slip) plus additional terms due to time-dependent slip $\delta(x,t)$ on the interface, in the form:

$$\tau(x,t) = \tau^{\mathrm{l}}(x,t) + f(x,t) - \frac{\mu}{2c_{\mathrm{s}}} V(x,t), \tag{3}$$

where $f(x,t)$ is a functional of slip history on the interface and $V(x,t) = \partial\delta(x,t)/\partial t$ is slip velocity. As $f(x,t)$ is obtained analytically through a closed-form Green function, boundary integral methods can be considered semi-analytical and tend to be more accurate than other numerical approaches such as finite difference methods (e.g., Day et al., 2005). $f(x,t)$ is related to $\delta(x,t)$ and history of $V(x,t)$ in the Fourier domain (Appendix B), and hence the spatial extent of the simulated interface is actually infinite with the domain of interest periodically replicated along the interface. The size of the domain is chosen so that waves from its periodic replications do not reach spatial locations of interest during the simulated time. Note that slip does not affect normal tractions $\sigma(x)$ which remain constant in this model.

Spontaneous rupture of the interface is simulated by requiring, at each time step, that shear traction (3) is equal to shear strength (2) for points along the interface that have non-zero slip velocity, and that shear traction (3) is smaller than shear strength (2) for points along the interface that have zero slip velocity. More details about the formulation and numerical procedure are given in Appendix B and Day et al. (2005).

Loading is incorporated in the model by prescribing traction $\tau^{\mathrm{l}}(x,t)$ in Eq. (3) that would act on the interface if it were constrained against any slip. $\tau^{\mathrm{l}}(x,t)$ is equal to a constant value, τ^o, on most of the interface. We call τ^o "background prestress" and quantify it in two ways. $\bar{\tau}^o = (\tau^o - \tau^{\mathrm{d}})/(\tau^{\mathrm{s}} - \tau^{\mathrm{d}})$ gives a non-dimensional value of τ^o which increases with τ^o. The seismic ratio $S = (\tau^{\mathrm{s}} - \tau^o)/(\tau^o - \tau^{\mathrm{d}})$ (Andrews, 1976) is smaller for larger τ^o. In a region close to $x=0$, $\tau^{\mathrm{l}}(x,t)$ is such that a main crack spontaneously spreads from there starting at $t=0$. $\tau^{\mathrm{l}}(x,t)$ is elevated above τ^o in a region of favorable heterogeneity of the size $2L_{\mathrm{h}}$ located at $x=D$ (Fig. 1). D is fixed and equal to $12L^{\mathrm{c}}$. Dependence of results on D is discussed in Section 4. Further specification of $\tau^{\mathrm{l}}(x,t)$ and the process of initiating the main crack are discussed in Sections 3 and 4.

Uenishi and Rice (2003) considered a quasi-static mode II crack on a linearly slip-weakening interface subjected to peaked loading. They demonstrated that the crack would become unstable when its half length reaches the nucleation half length given by

$$L^{\mathrm{nucl}} = \frac{0.579}{1-\nu}\frac{\mu d_0}{(\tau^{\mathrm{s}} - \tau^{\mathrm{d}})} = 0.579\pi\frac{(\tau^o - \tau^{\mathrm{d}})^2}{(\tau^{\mathrm{s}} - \tau^{\mathrm{d}})^2} L^{\mathrm{c}}, \tag{4}$$

assuming that the crack half length reaches L^{nucl} while slip inside the crack is still below d_0. In other words, L^{nucl} is relevant for cracks developing in such a way that their half length reaches L^{nucl} before their slip (or relative shear displacement) exceeds d_0. In that case, the entire crack length lies within the cohesive zone up until unstable crack propagation, and the singular crack theory cannot be used. As demonstrated by Uenishi and Rice (2003) and confirmed in this study, this situation is relevant for a wide range of loading conditions. We discuss the relation of L^{nucl} to our results in the following sections. Note that L^{nucl} could be chosen as

Table 1
Values of S, $L^{\mathrm{nucl}}/L^{\mathrm{c}}$, and numerical resolution of L^{c} and Λ_0 for different prestress levels τ^o

$\bar{\tau}^o = (\tau^o - \tau^{\mathrm{d}})/(\tau^{\mathrm{s}} - \tau^{\mathrm{d}})$	0.33	0.25	0.20	0.08
$S = (\tau^{\mathrm{s}} - \tau^o)/(\tau^o - \tau^{\mathrm{d}})$	2	3	4	11.5
$L^{\mathrm{nucl}}/L^{\mathrm{c}}$	0.202	0.114	0.073	0.012
$N^{\mathrm{c}} = L^{\mathrm{c}}/\Delta x$	100	100	100	800
$\Lambda_0/\Delta x$	30.8	17.4	11.1	14.2

$N^{\mathrm{c}} = 100$ is the lowest resolution used. Numerical convergence have been verified by considering N^{c} equal to 200, 400, and, in some cases, 1200, which increases the resolution of the cohesive zone by a factor of two, four, and 12, respectively.

a characteristic length scale in our models but we use the critical half length L^{c} in that capacity, to facilitate comparison with previous studies. As a reminder, $L^{\mathrm{c}} = (2\pi(1-\nu))^{-1}\mu G/(\tau^o - \tau^{\mathrm{d}})^2$ gives the half length for a singular crack, with fracture energy G and residual shear stress τ^{d}, which is in the critical state (such that, for an infinitesimal crack advance, the energy released is exactly balanced by the energy absorbed) under uniform far-field stress τ^o. L^{c} is relevant for cohesive-zone models of cracks in situations when the cohesive zone sizes at the crack tips of quasi-static cracks are small compared to the overall crack size, which means that cracks are still quasi-static when slip exceeds d_0 over most of the crack length. Note that L^{nucl} is independent of background prestress τ^o but the normalized ratio $L^{\mathrm{nucl}}/L^{\mathrm{c}}$ depends on τ^o (Table 1).

Rupture propagation is simulated on a uniform spatial grid with the cell size $\Delta x = L^{\mathrm{c}}/N^{\mathrm{c}}$ and constant time step $\Delta t = \Delta x/(\beta c_{\mathrm{s}})$, where N^{c} is the number of cells in the length L^{c}, and β determines the time step as a fraction (equal to $1/\beta$) of the time for the shear wave to travel through Δx. An important quantity to resolve is the cohesive zone length at the crack tip (Palmer and Rice, 1973; Day et al., 2005). A useful upper bound for the cohesive zone length of a sub-Rayleigh crack is given by the cohesive zone length Λ_0 of a crack propagating at 0^+ speeds (Palmer and Rice, 1973; Rice, 1980):

$$\Lambda_0 = \frac{9\pi}{32(1-\nu)}\frac{\mu d_0}{(\tau^{\mathrm{s}} - \tau^{\mathrm{d}})}. \tag{5}$$

Note that, for given friction properties, L^{nucl} and Λ_0 differ only by a prefactor of order 1. Table 1 relates numerical resolution of L^{c} and Λ_0 and gives values of $L^{\mathrm{nucl}}/L^{\mathrm{c}}$ for different prestress levels τ^o used in this study.

We use the following non-dimensional variables: time $\bar{t} = c_{\mathrm{s}}t/L^{\mathrm{c}}$, length $\bar{x} = x/L^{\mathrm{c}}$, slip velocity $\bar{V} = \mu V/c_{\mathrm{s}}(\tau^o - \tau^{\mathrm{d}})$, and stress $\bar{\tau} = (\tau - \tau^{\mathrm{d}})/(\tau^{\mathrm{s}} - \tau^{\mathrm{d}})$. All other variables and quantities are non-dimensionalized accordingly and their non-dimensional names are denoted by adding a bar "-". For example, $\bar{\tau}^o = (\tau^o - \tau^{\mathrm{d}})/(\tau^{\mathrm{s}} - \tau^{\mathrm{d}})$ and $\bar{L}^{\mathrm{nucl}} = L^{\mathrm{nucl}}/L^{\mathrm{c}}$. Note that $\bar{\tau}^{\mathrm{s}} = 1$, $\bar{\tau}^{\mathrm{d}} = 0$, and $\bar{L}^{\mathrm{c}} = 1$. For clarity, we sometimes specify non-dimensional quantities in terms of their dimensional analogs.

Slip progression along the interface is tracked using the notion of rupture time. Non-dimensional rupture time is defined as the non-dimensional time $\bar{t}(\bar{x})$ when slip rate $\bar{V}$ of point $\bar{x}$ becomes non-zero for the first time. Our implementation of that definition is to require that slip rate exceeds a given small value, $\bar{V}_{\mathrm{c}}$. The results do not depend on the value of $\bar{V}_{\mathrm{c}}$ as long as it is small enough to capture slip initiation. We adopt $\bar{V}_{\mathrm{c}} = 10^{-6}$. Note that, for $\mu = 3 \times 10^4$ MPa and $c_{\mathrm{s}} = 3 \times 10^3$ m/s typical for rocks, and $\tau^o - \tau^{\mathrm{d}} = 10$ MPa which is the order of magnitude for typical stress drops during large earthquakes, $\bar{V}_{\mathrm{c}} = 10^{-6}$ corresponds to the dimensional value of 10^{-6} m/s. In all cases we checked, we find that any spatial cell with non-zero slip rate has non-dimensional slip rate larger than 10^{-6}, which means that this choice for $\bar{V}_{\mathrm{c}}$ appropriately captures initiation of slip.

3. Advancing main rupture towards a preexisting subcritical crack: an example of abrupt sub-Rayleigh-to-intersonic transition

To smoothly initiate a main crack and a subcritical secondary crack, we conduct a preliminary quasi-dynamic calculation in which the part of the functional $f(x,t)$ that accounts for wave mediated stress transfers

is ignored (Appendix B). We prescribe loading traction $\bar{\tau}^{\mathrm{l}}(\bar{x},\bar{t}')$ which has two peaks, at $\bar{x}=0$ and $\bar{x}=\bar{D}$:

$$\bar{\tau}^{\mathrm{l}}(\bar{x},\bar{t}')=\bar{\tau}^{o}+(1-\bar{\tau}^{o})(1+R\bar{t}')\left\{\exp\left[-\left(\frac{\bar{x}}{\bar{L}^{\mathrm{nucl}}}\right)^{2}\right]+\exp\left[-\left(\frac{\bar{x}-\bar{D}}{\bar{L}^{\mathrm{nucl}}/2}\right)^{2}\right]\right\}. \tag{6}$$

In Eq. (6), R is the loading rate of the imposed peaks and $\bar{\tau}^{o}$ is (constant) background prestress outside of the two peaks; $\bar{\tau}^{o}=0.33$ (i.e., $S=2$) in this section. At $\bar{t}'=0$, frictional sliding initiates at $\bar{x}=0$ and $\bar{D}$. We let the sliding zone centered at $\bar{x}=0$ expand until it reaches a certain half size $\bar{L}_{\mathrm{ini}}$. This happens at the time $\bar{t}'=\bar{t}'_{\mathrm{ini}}$. We save the corresponding distributions of loading tractions $\bar{\tau}^{\mathrm{l}}$, shear tractions $\bar{\tau}$, slip $\bar{\delta}$, and slip velocity $\bar{V}$ along the interface, and use them as initial conditions for a subsequent fully dynamic calculation, in which we reset the time by setting $\bar{t}=\bar{t}'-\bar{t}'_{\mathrm{ini}}$. Note that loading tractions $\bar{\tau}^{\mathrm{l}}(\bar{x},\bar{t})$ are unchanged thereafter (for all $\bar{t}>0$).

We choose parameters of the initiation procedure that mimic tectonically driven slow nucleation on faults in the Earth's crust and result in smooth acceleration of the main crack. For that, we first consider the initiation of the main crack separately, without the second exponential term in Eq. (6). We consider progressively slower loading rates $R=0.63$, 0.063, and 0.0063 and progressively smaller initial half sizes $\bar{L}_{\mathrm{ini}}=\bar{L}^{\mathrm{nucl}}$, $0.9\bar{L}^{\mathrm{nucl}}$, and $0.8\bar{L}^{\mathrm{nucl}}$ and compare stress conditions that the resulting main crack creates at the location $\bar{x}=\bar{D}=12$ of the preexisting subcritical crack. For $\bar{L}_{\mathrm{ini}}=\bar{L}^{\mathrm{nucl}}$, loading rates $R=0.063$ and 0.0063 give virtually identical stressing conditions as shown in Fig. 3; we use $R=0.0063$ in the simulations described in this work. For $R=0.0063$, $\bar{L}_{\mathrm{ini}}=0.8\bar{L}^{\mathrm{nucl}}$ does not initiate spontaneous crack propagation, while both $\bar{L}_{\mathrm{ini}}=0.9\bar{L}^{\mathrm{nucl}}$ and $\bar{L}_{\mathrm{ini}}=\bar{L}^{\mathrm{nucl}}$ create a spontaneously propagating main crack that smoothly accelerates from near-zero tip speeds. $\bar{L}_{\mathrm{ini}}=0.9\bar{L}^{\mathrm{nucl}}$ and $\bar{L}_{\mathrm{ini}}=\bar{L}^{\mathrm{nucl}}$ result in virtually indistinguishable stressing conditions at the location of the subcritical crack. We choose $\bar{L}_{\mathrm{ini}}=\bar{L}^{\mathrm{nucl}}$ because it results in shorter computation time. The importance of the initiation procedure and related results of Festa and Vilotte (2006), Shi et al. (2007), and Geubelle and Kubair (2001) are discussed in Section 5.4.

The shear stress distribution at the beginning of a dynamic simulation is shown in Fig. 4. At $\bar{t}=0$, the secondary crack centered at $\bar{x}=12$ is much smaller than the main crack (which has length $\bar{L}^{\mathrm{nucl}}$), constituting a subcritical crack. The background prestress level $\bar{\tau}^{o}=0.33$ is below the critical value 0.36 of the Burridge–Andrews mechanism. $\bar{\tau}^{o}=0.33$ is even lower if compared to the value $\bar{\tau}_{\mathrm{BA}}=0.53$ needed for the Burridge–Andrews transition at the location $\bar{x}=13.5$ which is close to the location of the subcritical crack. Hence no intersonic transition would occur under such prestress in the homogeneous case (with no preexisting subcritical crack).

For $\bar{t}>0$, the spontaneously propagating main crack sends out dilatational and shear waves, which impose an intersonic loading stress field (Appendix A) on the secondary subcritical crack. Fig. 5 (left panel) shows

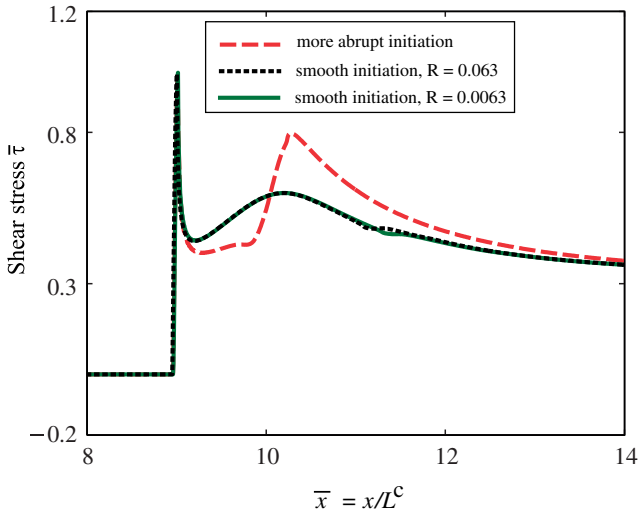

Fig. 3. Stress distribution on the interface for different initiation procedures. To compare stress fields created by the main crack, no heterogeneity at $\bar{x}=12$ is imposed for these simulations. The more abrupt initiation procedure that results in a higher shear stress peak is discussed in Section 4.

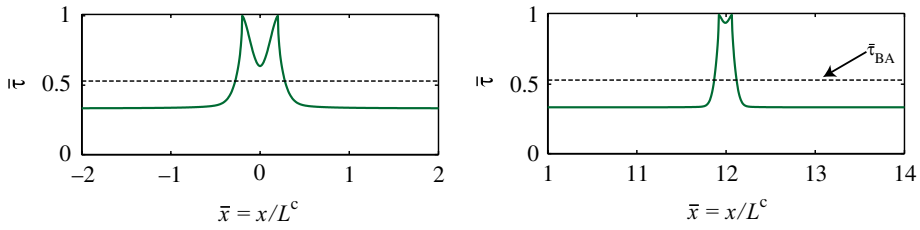

Fig. 4. Stress distribution around the main crack and preexisting subcritical crack at $\bar{t} = 0$ (solid green line). The main crack centered at $\bar{x} = 0$ is poised to propagate spontaneously for $t > 0$, while the secondary crack centered at $x = 12L^c$ remains a subcritical crack. Prestress outside of zones affected by cracks is equal to $\bar{\tau}^o = 0.33$. $\bar{\tau}_{BA} = 0.53$ (black dashed line) is the prestress level required for intersonic transition at the location $\bar{x} = 13.5$ by the Burridge–Andrews mechanism.

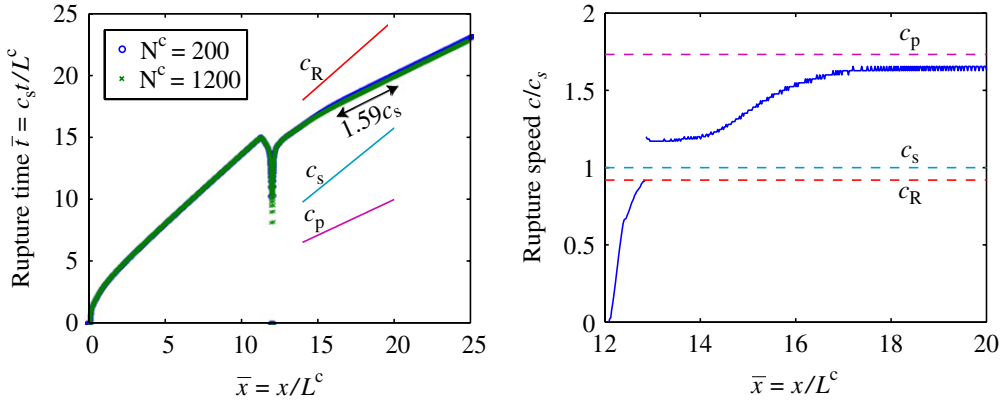

Fig. 5. Left panel: rupture time along the interface for the case with a preexisting subcritical crack. Under the stress field of the advancing main crack, the secondary subcritical crack begins to spread at $\bar{t} = c_s t/L^c = 7.9$ and eventually propagates with intersonic speeds. Note that the results of simulations with two resolutions, $N^c = 200$, $\beta = 4$ and $N^c = 1200$, $\beta = 4$, are almost indistinguishable on the scale of the plot. More resolution comparisons are shown in Fig. 6. Right panel: rupture speed of the secondary crack. It approaches the Rayleigh-wave speed and then abruptly jumps to intersonic speeds. Rupture speed is determined for the case with resolution $N^c = 1200$, $\beta = 4$ by dividing the interface into intervals of 24 cells each, computing average rupture speed over each interval, and plotting the obtained value with respect to the middle of the interval. Care is taken to make the location of the rupture speed jump correspond to a beginning or end of an interval.

rupture time on the interface. The secondary crack begins to spread at the time $\bar{t} = c_s t/L^c = 7.9$ with rupture speeds close to zero. At that time, the main crack tip arrives at the position $5.4L^c$. As the main crack approaches, the secondary crack rapidly accelerates to the Rayleigh wave speed c_R and then jumps to an intersonic speed (Fig. 5, right panel). The crack tip speed of the secondary crack before the jump is numerically indistinguishable from c_R, so it is possible that the crack tip speed reaches c_R momentarily before the jump. Note that while steady crack propagation with c_R would result in zero cohesive zone length and infinite slip velocities and hence would be impossible, transient propagation with c_R cannot be excluded.

To confirm the abrupt nature of the sub-Rayleigh-to-intersonic transition of the secondary crack, we have done simulations with several levels of resolution, from $N^c = 200$, $\beta = 4$ to $N^c = 1200$, $\beta = 4$. Fig. 6 shows the space–time progression of the rupture front of the secondary crack close to the location and time of the transition. The results have converged with respect to the discretization of space and time. For example, the location of the transition is 12.862 for $N^c = 800$ and 12.855 for $N^c = 1200$, a relative difference of less than 0.1%. As Fig. 6 demonstrates, the sub-Rayleigh-to-intersonic transition occurs within one spatial grid cell Δx and one time step Δt for all resolutions we have considered. Hence, in the limit of $\Delta x \to 0$ and $\Delta t \to 0$, the crack tip should abruptly jump from c_R to an intersonic speed.

Fig. 7 illustrates abrupt transition of the secondary crack tip to intersonic speeds by giving snapshots of slip velocity and stress distributions at the crack tip. At time $\bar{t} = c_s t/L^c = 15.02$, the tip of the secondary crack propagates with the speed numerically equal to c_R. At $\bar{t} = 15.04$, sliding initiates just *one* cell ahead of the

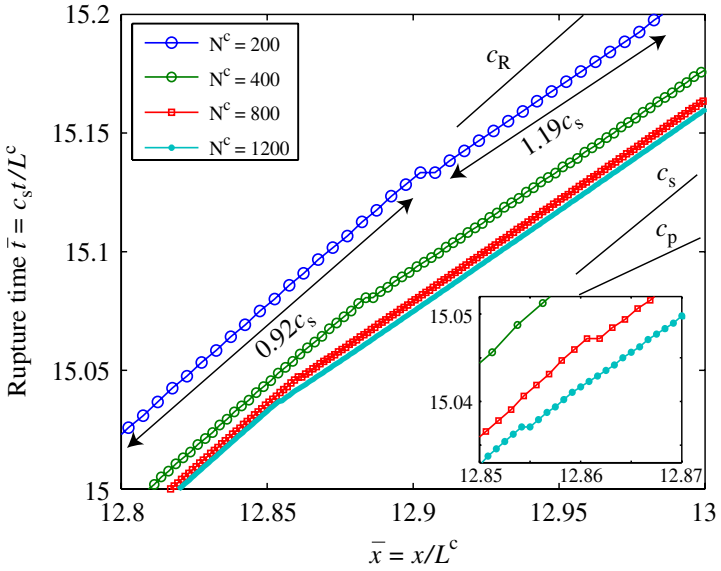

Fig. 6. Propagation of the secondary crack in the region where sub-Rayleigh-to-intersonic transition occurs. Rupture time of each spatial cell is indicated using different symbols for different resolution. For progressively finer resolution (i.e., larger N^c), transition occurs within one cell size Δx and one time step Δt, which means that, in the limit of $\Delta x \to 0$ and $\Delta t \to 0$, the rupture front abruptly jumps from speeds numerically equal to $c_R = 0.92c_s$ to an intersonic speed.

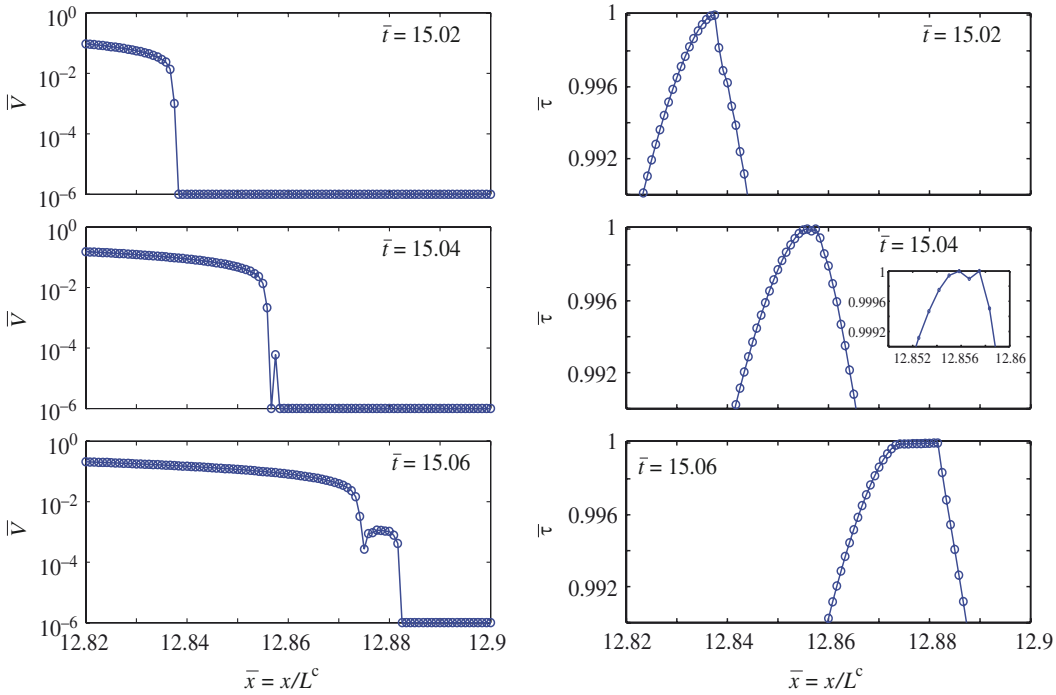

Fig. 7. Snapshots of slip velocity (left) and shear stress distributions (right) on the interface during sub-Rayleigh-to-intersonic transition for the case $N^c = 1200$, $\beta = 4$, zooming in on the crack tip. Slip velocity is plotted on the logarithmic scale. For plotting convenience, slip velocity shown is the actual slip velocity plus 10^{-6} and hence zero slip velocity appears as 10^{-6} on the plot. At time $\bar{t} = c_s t/L^c = 15.02$, the crack tip propagates with the speed numerically equal to c_R. At $\bar{t} = 15.04$, sliding initiates just *one* cell ahead of the crack tip and propagates with intersonic speeds.

crack tip and the sliding region propagates with intersonic speeds immediately. This process is the same in simulations with different Δx and time step Δt. In the limit of $\Delta x \to 0$ and $\Delta t \to 0$, intersonic sliding should be inseparable from the crack tip, and initiate exactly at the tip.

Hence we conclude that the secondary crack transitions from sub-Rayleigh to intersonic speeds by abruptly changing the speed of its tip. This transition mechanism is different from the Burridge–Andrews mechanism, in which a daughter crack starts out as an intersonic crack. Note that once the secondary crack transitions to intersonic speeds, it accelerates to speeds close to c_p and maintains them for long propagation distances. Further discussion of this mechanism is given in Section 5.1 and Appendix C. Whether the transition occurs or not should depend on the size of the preexisting crack, background prestress $\bar{\tau}^o$, and loading provided by the main crack. (The loading significantly depends on the initiation procedure for the main crack, as explained in Sections 4 and 5.4.) We explore these dependencies for a related case of a patch of higher prestress discussed in the next section.

4. Advancing main crack towards a patch of higher prestress: dependence on patch size, prestress, and location

Instead of a preexisting crack (Section 3), let us consider higher prestress $\bar{\tau}^o_h = (\tau^o_h - \tau^d)/(\tau^s - \tau^d)$ in a small patch $\bar{D} < \bar{x} < \bar{D} + 2\bar{L}_h$, where $\bar{L}_h = L_h/L^c$ is the half size of the patch (Fig. 8). We select $\bar{D} = 12$. Sliding in the patch starts from its end $\bar{x} = \bar{D}$ (closer to the main crack) at the same time for all patch sizes, everything else being equal. We use two ways to initiate the main crack: (i) the same smooth initiation as in Section 3, and (ii) a more abrupt initiation for which, at $\bar{t} = 0$, prestress within $|\bar{x}| < 1$ is set to be 1% larger than the static strength τ^s of the interface. In the case of (ii), the main crack initiates at once in the entire region $|\bar{x}| < 1$. It accelerates and acquires speeds close to c_R much sooner than in the case of the smooth initiation procedure. This results in a significantly higher shear stress peak as shown in Fig. 3. For the smooth initiation, such a shear stress peak would result only after much longer rupture propagation along the interface. As in Section 3, background prestress $\bar{\tau}^o$ is chosen low compared to prestress required for intersonic transition by the Burridge–Andrews mechanism. If there were no patch of higher prestress, no intersonic transition and propagation would occur.

Spontaneous propagation of the main crack for times $\bar{t} > 0$ imposes an additional dynamic stress field on the patch of higher prestress. For a range of patch sizes L_h/L^c and values of background prestress $\bar{\tau}^o_h$, as discussed in the following, shear stress in the patch overcomes the static friction strength τ^s before the arrival of the shear stress peak, and secondary sliding (or crack) initiates at the patch corner $\bar{x} = 12$ closest to the main crack. The secondary crack spreads along the patch with intersonic speeds, driven by intersonic stress increase due to the advancing main crack. So far, the behavior is intuitively obvious. However, it is not intuitively clear how this intersonic secondary crack would behave after it enters the surrounding region of lower background prestress. While intersonic propagation over the higher-stressed patch is an interesting phenomenon, we would like to study whether the patch can induce sustained intersonic propagation for long distances beyond the patch. Hence in the following we call "sub-Rayleigh" those scenarios that result in the eventual sub-Rayleigh propagation of the crack, despite the fact that all scenarios include intersonic propagation of the secondary crack over the higher-stressed patch.

Our simulations show that behavior of the secondary crack after it leaves the patch of higher prestress is quite complicated. First, its tip speed momentarily reduces to zero, at least for small patch sizes studied here. Its subsequent behavior depends on background prestress $\bar{\tau}^o$, on the additional loading provided by the main crack, on the level $\bar{\tau}^o_h$ of prestress in the patch, and on the patch size $\bar{L}_h = L_h/L^c$. Loading provided to the

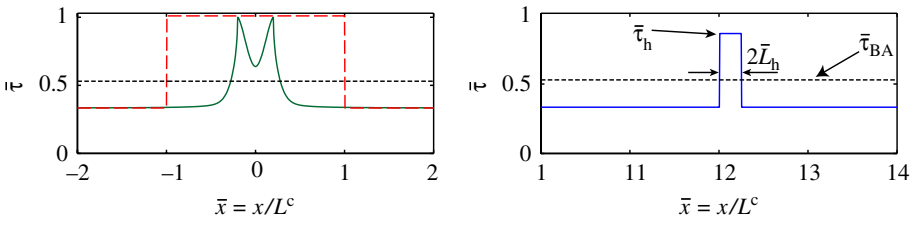

Fig. 8. Shear stress distribution around the main crack (left panel) and the patch of higher prestress (right panel) at $\bar{t} = 0$ ($\bar{\tau}^o = 0.33$). In the left panel, the solid green and dashed red lines correspond to the smooth and more abrupt initiation procedures, respectively. $\bar{\tau}_{BA} = 0.53$ is the level of prestress required to achieve Burridge–Andrews intersonic transition at the location $\bar{x} = 13.5$ with the smooth initiation procedure.

patch by the main crack depends on background prestress $\bar{\tau}^o$, the position of heterogeneity $\bar{D}$, and the procedure of main crack initiation. For each initiation procedure, we fix $\bar{D} = 12$ and consider the dependence of results on the patch prestress $\bar{\tau}^o_h$ and size $\bar{L}_h$ for different values of $\bar{\tau}^o$. Intuitively, the larger the patch and the higher prestress it has, the more likely it is to cause transition to intersonic speeds. Yet the simulation results are more complex.

We start by describing results for the more abrupt initiation (ii) of the main crack. Results of our simulations in terms of intersonic vs. sub-Rayleigh propagation of rupture beyond the patch of higher prestress are summarized in Fig. 9. To determine the eventual crack speed, we simulate rupture propagation until the location $\bar{x} = x/L^c = 16$ is ruptured. For cases that require further clarification, and for selected conceptually important cases, we redo calculations until the location $\bar{x} = 25$ is ruptured. Note that our methodology periodically repeats the simulated domain. Hence, to simulate a bilateral main crack and to avoid waves arriving from periodic replications of the rupture process into the region of observation, we use domain lengths of 50 and 80 to determine the crack speed at locations $\bar{x} = 16$ and 25, respectively.

Fig. 9 (top panel) shows results for $\bar{\tau}^o = 0.25$ ($S = 3$). We find two regions of sub-Rayleigh behavior, marked "Sub-Rayleigh I" and "Sub-Rayleigh II" in the figure, and one connected region of intersonic behavior. Boundaries separating regions of intersonic and sub-Rayleigh behavior are approximate in Fig. 9, inferred based on simulated cases shown as dots. We have studied many cases close to the boundaries, and

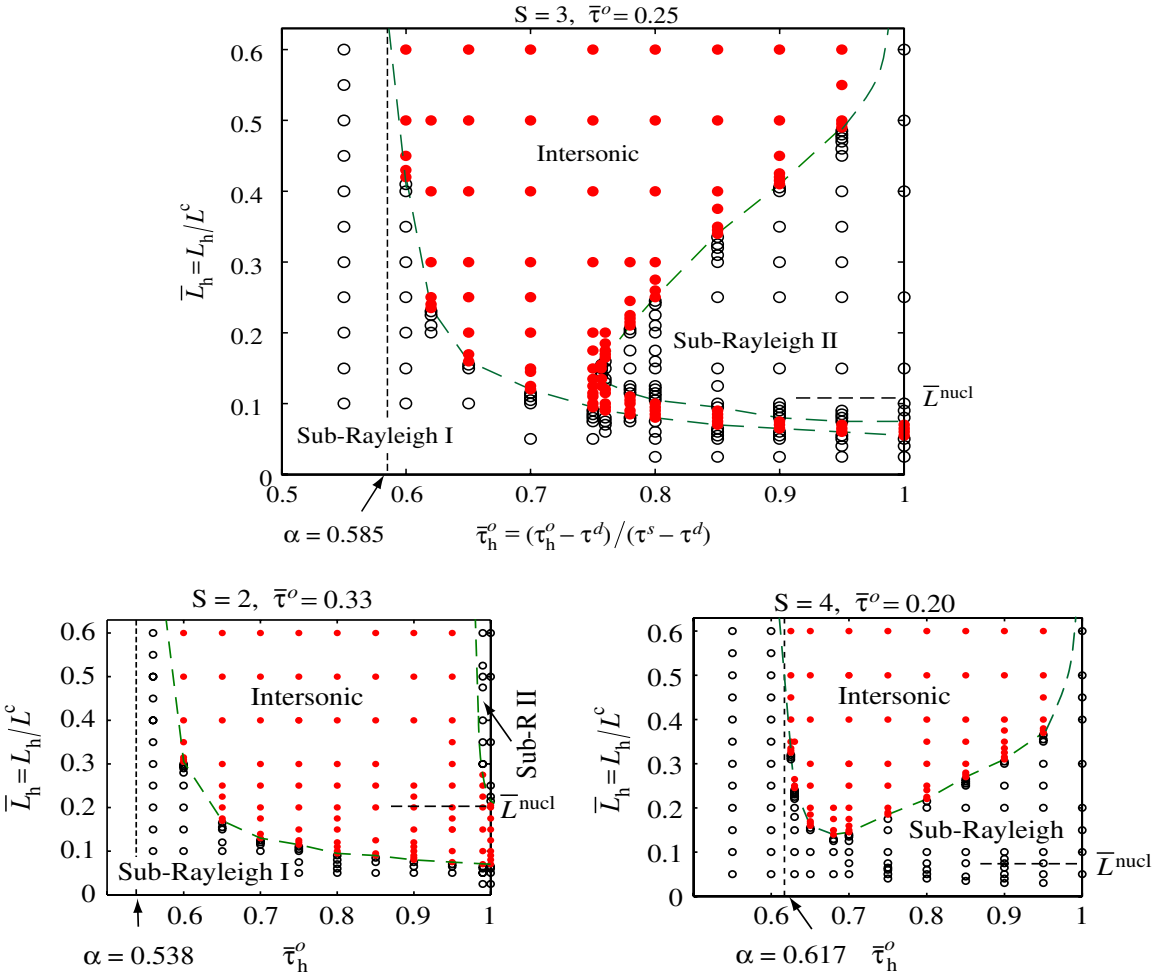

Fig. 9. Influence of patch parameters on eventual intersonic vs. sub-Rayleigh propagation for three different values of background prestress and more abrupt initiation of the main crack. The horizontal and vertical axes indicate the patch prestress and patch size, respectively. Red filled dots indicate simulated cases for which rupture has sustained intersonic speeds beyond the higher-stressed patch. Black open dots indicate simulated cases for which rupture stays sub-Rayleigh. Dashed green lines indicate approximate boundaries of different behavior. The value α of the patch prestress is discussed in the text.

that is why dots close to the boundaries overlap. Results for cases $\bar{\tau}^o = 0.33$ ($S = 2$) and $\bar{\tau}^o = 0.2$ ($S = 4$) are shown in Fig. 9, bottom panels. Comparison of cases $\bar{\tau}^o = 0.25$ and 0.33 shows that regions of sub-Rayleigh behavior shrink for the higher background prestress $\bar{\tau}^o = 0.33$, especially region "Sub-Rayleigh II". Comparison of cases $\bar{\tau}^o = 0.25$ and 0.2 shows that for the lower background prestress $\bar{\tau}^o = 0.2$, regions of sub-Rayleigh behavior expand and overlap, creating a single larger sub-Rayleigh region. Hence larger background prestress favors intersonic propagation, as could be expected, and causes consistent motion of the boundaries separating sub-Rayleigh and intersonic behavior.

Simulations for the smooth main crack initiation, which results in a smaller shear stress peak as the main crack approaches the patch of higher prestress, are summarized in Fig. 10. We see qualitatively similar behavior in terms of where regions of sub-Rayleigh and intersonic propagation are located. As could be expected, a smaller shear stress peak results in smaller regions of intersonic propagation for the same values of background prestress.

To explain the existence and location of regions of sub-Rayleigh and intersonic behavior in Figs. 9 and 10, let us consider some limiting cases. If there were no patch of higher prestress, the main crack would stay sub-Rayleigh, as all background prestress values $\bar{\tau}^o$ considered here are lower than prestress required for transition by the Burridge–Andrews mechanism. A very small patch should have the same effect as no patch, and hence we should have sub-Rayleigh propagation for patch half sizes $\bar{L}_h = L_h/L^c$ close to zero, regardless of the patch prestress. This explains the existence of the region marked "Sub-Rayleigh I" close to the $\bar{L}_h = 0$ line for any value of $\bar{\tau}^o_h$. For most cases in region "Sub-Rayleigh I", the main crack overtakes secondary sliding, and continues its sub-Rayleigh propagation. An example of such case is shown in Fig. 11 (left panel, $\bar{L}_h = 0.055 = 0.48\bar{L}^{nucl}$). Only for cases close to the boundary with the intersonic region, the secondary crack either just manages to propagate with sub-Rayleigh speed itself, or even transitions to intersonic speeds for a brief time and then reverts back to sub-Rayleigh speeds (Fig. 11, right panel).

If the prestress level in the patch is equal to the static strength, $\bar{\tau}^o_h = 1$, then secondary sliding starts in the patch at $\bar{t} = 0$, when the main crack is still far away. If the patch is large enough, as approximately given by $\bar{L}_h \geqslant \bar{L}^{nucl}$, then the secondary crack develops into a spontaneous sub-Rayleigh crack and runs away with speeds close to c_R before the main crack can approach and interact with that process. Similar behavior occurs for $\bar{\tau}^o_h$ close to 1. Case $\bar{L}_h = 0.2 = 1.75\bar{L}^{nucl}$, $\bar{\tau}^o_h = 0.85$ in Fig. 11 is an example of such behavior. This argument explains the existence of the region marked "Sub-Rayleigh II" which includes a part of the line $\bar{\tau}^o_h = 1$.

If the patch with $\bar{\tau}^o_h = 1$ is small, as approximately given by $\bar{L}_h \leqslant \bar{L}^{nucl}$, then it develops into a subcritical crack and, similarly to the preexisting crack case of Section 3, such subcritical cracks can be driven, under the right conditions, to intersonic speeds by the stress field of the advancing main crack. Such intersonic cases separate the two sub-Rayleigh regions for background prestress values $\bar{\tau}^o = 0.25$ and 0.33 in Fig. 9 and

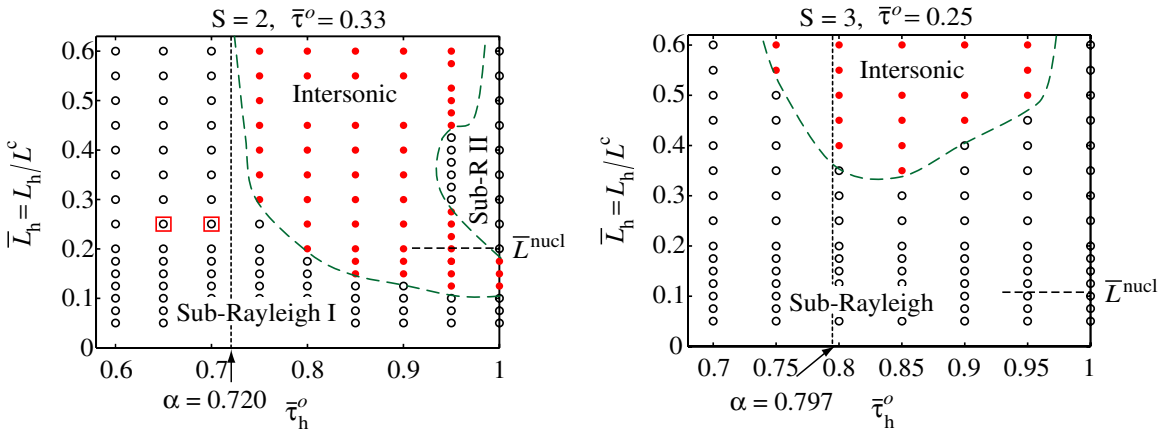

Fig. 10. Influence of patch parameters on intersonic vs. sub-Rayleigh propagation for smooth initiation of the main crack that results in a smaller shear stress peak. The horizontal and vertical axes indicate the patch prestress and patch size, respectively. Red filled dots indicate simulated cases for which rupture has sustained intersonic speeds beyond the higher-stressed patch. Black open dots indicate simulated cases for which rupture stays sub-Rayleigh. Dashed green lines indicate approximate boundaries of different behavior. The value α of the patch prestress, and two cases marked by small red squares are discussed in the text.

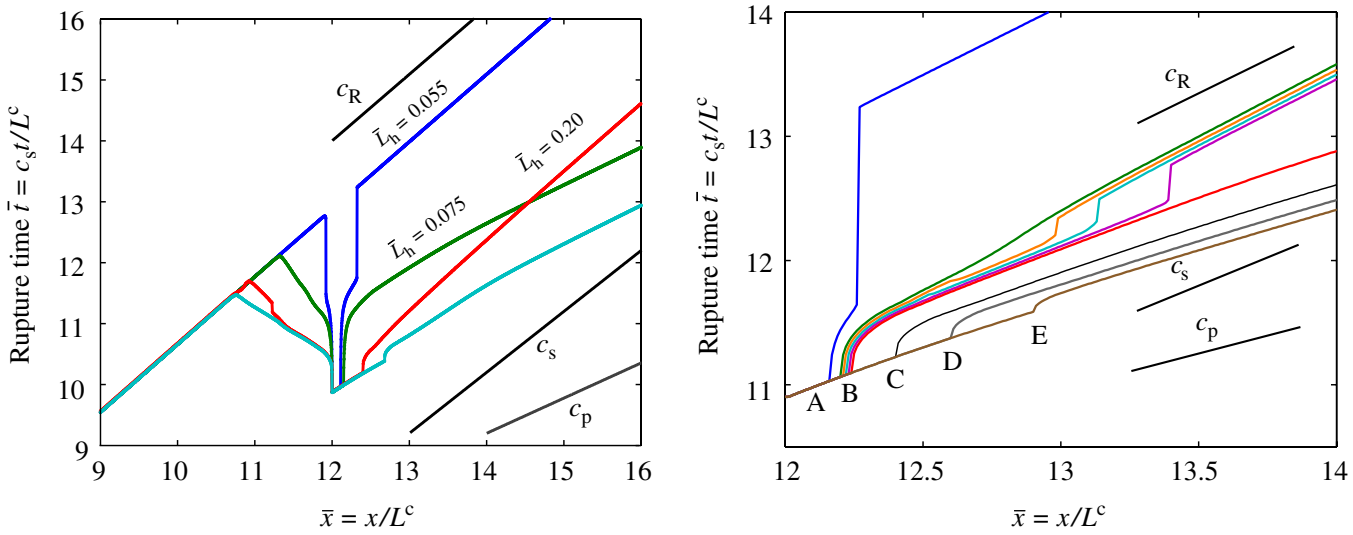

Fig. 11. Rupture time for different patch sizes, with $\bar{\tau}^o = 0.25$ ($S = 3$) and more abrupt initiation of the main crack. Left panel: patch prestress $\bar{\tau}^o_h = 0.85$. Rupture eventually propagates with intersonic speeds for $\bar{L}_h = L_h/L^c = 0.075$ and 0.34 and sub-Rayleigh speeds for $\bar{L}_h = 0.055$ and 0.20. Behavior for these and other patch sizes is discussed in the text. Right panel: patch prestress $\bar{\tau}^o_h = 0.70$, note a different scale of $\bar{x}$. The behavior is much simpler than for $\bar{\tau}^o_h = 0.85$. Cases with different $\bar{L}_h$ are marked by letters A–E at the location $\bar{x} = 12 + 2\bar{L}_h$ where the secondary crack for each case leaves the patch. $\bar{L}_h = 0.08$, line A: the secondary crack is overtaken by the main crack for this and smaller $\bar{L}_h$. $\bar{L}_h = 0.1, 0.105, 0.11, 0.115, 0.12$, lines B: for $0.1 \leqslant \bar{L}_h \leqslant 0.115$, the secondary crack accelerates to c_R and abruptly transitions to intersonic speeds, but reverts back to sub-Rayleigh speeds after short (but progressively longer) intersonic propagation; for $\bar{L}_h = 0.12$, the crack manages to stay intersonic and results in eventual intersonic propagation. $\bar{L}_h = 0.20, 0.30, 0.45$, lines C–E: same behavior as for $\bar{L}_h = 0.12$.

$\bar{\tau}^o = 0.33$ in Fig. 10. An example of such intersonic behavior is the case of $\bar{L}_h = 0.075 = 0.66\bar{L}^{nucl}$ in Fig. 11. However, regions "Sub-Rayleigh I" and "Sub-Rayleigh II" merge for lower levels of background prestress and smaller shear stress peaks, as Figs. 9 and 10 show. The resulting connected sub-Rayleigh region consists of two distinct areas, one in which the eventual sub-Rayleigh propagation is due to the main crack, and the other in which the eventual sub-Rayleigh propagation is due to the secondary crack. Note that large patches (i.e., larger than L^{nucl}) with uniform prestress $\bar{\tau}^o_h = 1$ (or close to 1) are unlikely to exist on the path of another crack in a realistic situation (i.e., on faults in the Earth's crust). Any small heterogeneities or perturbations would lead to development of unstable sliding in those patches, effectively nucleating a main crack there. Such patches are considered in this study mostly to have a better understanding of the parameter space.

If the shear stress peak traveling in front of the main crack does not initiate sliding in the patch, lower shear stresses behind the peak cannot do that either, and sliding in the patch initiates only due to high stresses very close to the main crack tip. In this situation, a small patch can no longer create a preexisting subcritical crack that could be driven to intersonic speeds by the approaching main crack. Hence small patches can only cause intersonic transition for large enough values of the patch prestress, $\bar{\tau}^o_h > \alpha$, where α is the patch prestress which would be brought to the static strength by the maximum of the shear stress peak. Prestress α satisfies $1 - \alpha = \bar{\tau}^{peak} - \bar{\tau}^o$, where $\bar{\tau}^{peak}$ is the maximum of the shear stress peak when it arrives at the patch. The value of $\bar{\tau}^{peak}$ depends on the history of the main crack; in our simulations, it is determined by the initiation procedure, background prestress, and location of the patch (which is fixed at $\bar{x} = 12$). For $\bar{\tau}^o = 0.25$ ($S = 3$) and more abrupt initiation of the main crack, simulations show that $\bar{\tau}^{peak} = 0.665$, which leads to $\alpha = 0.585$. The values of α for other values of $\bar{\tau}^o$ and for smooth initiation of the main crack are determined analogously. Lines $\bar{\tau}^o_h = \alpha$ are marked in Figs. 9 and 10 as vertical black lines with short dashes. Intersonic transition should be inhibited for $\bar{\tau}^o_h < \alpha$, at least for small patches, and that is what we observe in Figs. 9 and 10.

For patches with $\bar{\tau}^o_h > \alpha$, intersonic loading stress provided by the main crack creates intersonic secondary crack in the patch. When the intersonic secondary crack exits from the patch into the region of lower background prestress, it slows down first but, for large enough patch sizes, accelerates back at once and jumps abruptly to intersonic speeds (e.g., case $\bar{L}_h = 0.34 = 2.98\bar{L}^{nucl}$ in Fig. 11). That behavior can be understood as follows. Intersonic propagation in the patch radiates stress waves and most of them are left behind by the

intersonic secondary crack. When the secondary crack exits the patch and slows down, the stress field radiated by sliding in the patch catches up with the secondary crack and loads it. The duration of this loading depends on the patch size, and hence it would be increasingly important for larger patches, causing acceleration of the secondary crack and transition to intersonic speeds. Note that for patches with prestress lower than α but close to it, sliding in the patch is still intersonic but it is separated from the main crack only by a few cell sizes, and the behavior of the two cracks after exiting the patch cannot be well separated. Subsequent sustained intersonic propagation occurs only for large enough patches, as it is driven exclusively by stress radiation from the patch. For patch prestress levels much smaller than α, the main crack and secondary sliding in the patch cannot be separated, and the only effect of the patch is to increase the sub-Rayleigh propagation speed of the main crack.

More abrupt initiation of the main crack results in a larger shear stress peak and hence should provide an approximate picture of the model behavior for a patch located much farther from the initiation of the main crack (i.e., for larger $\bar{D}$). Consider the case of $\bar{\tau}^o = 0.33$. Through simulations we find that the more abrupt initiation procedure results in the same maximum of the shear stress peak at the location of $\bar{x} = 12$ as the smooth initiation procedure at the location of $\bar{x} = 80$. Given the high resolution we would like to achieve in this study, such long propagation distances are hard to study even in 2D. To check the correspondence between the smooth initiation procedure with $\bar{D} = 80$ and abrupt initiation procedure with $\bar{D} = 12$, we have done simulations with the smooth initiation procedure where we put a patch of higher prestress $\bar{\tau}^o_{\mathrm{h}} = 0.65$ or 0.7 and size $\bar{L}_{\mathrm{h}} = 0.25$ at the location $\bar{D} = 80$, with background prestress $\bar{\tau}^o = 0.33$ ($S = 2$). These cases are sub-Rayleigh for $\bar{D} = 12$ and smooth initiation (Fig. 10, left panel, open black dots surrounded by red squares). However, they are intersonic for $\bar{D} = 12$ and more abrupt initiation (Fig. 9, bottom left panel). For smooth initiation and $\bar{D} = 80$, these cases are also intersonic, indicating that more abrupt initiation and its higher shear stress peak can indeed approximate long propagation distances for the smooth initiation. The correspondence cannot be exact, however, since the shear stress distribution in front of the main crack keeps extending in space for longer propagation distances; the height of the peak may be the same, but its width would be different. Since the intersonic vs. sub-Rayleigh behavior depends not just on the stress field ahead of the main crack but also on other factors such as, for example, the patch size in relation to $\bar{L}^{\mathrm{nucl}}$, this discrepancy cannot be resolved by simply scaling the patch size in accordance with its location.

We have demonstrated that a small patch of higher prestress can completely change rupture behavior. To illustrate the complexity of the response that results when the stress field of the main crack interacts with the patch, let us consider the case of background prestress $\bar{\tau}^o = 0.25$ ($S = 3$), patch prestress $\bar{\tau}^o_{\mathrm{h}} = 0.85$, and more abrupt initiation of the main crack (Fig. 9, top panel). Rupture times for four values of the patch size $\bar{L}_{\mathrm{h}} = L_{\mathrm{h}}/L^{\mathrm{c}}$ are shown in Fig. 11 (left panel) but more cases (shown as dots in Fig. 9 for $\bar{\tau}^o_{\mathrm{h}} = 0.85$) are enumerated in the following. Note that $\bar{L}^{\mathrm{nucl}} = 0.11$ in this case.

For $\bar{L}_{\mathrm{h}} \leqslant 0.06$, the main crack overtakes the secondary crack, and continues its sub-Rayleigh propagation beyond the patch of higher stress (Fig. 11, $\bar{L}_{\mathrm{h}} = 0.055$). For $\bar{L}_{\mathrm{h}} = 0.065$, the secondary crack survives but stays sub-Rayleigh. For $0.07 \leqslant \bar{L}_{\mathrm{h}} \leqslant 0.085$, the secondary crack accelerates after a pause and acquires sustained intersonic speeds by the abrupt transition mechanism described in Section 3 (Fig. 11, $\bar{L}_{\mathrm{h}} = 0.075$). For $0.09 \leqslant \bar{L}_{\mathrm{h}} \leqslant 0.105$, the secondary crack accelerates to sub-Rayleigh speeds and creates an intersonic daughter crack in front; the daughter crack subsequently dies and the secondary crack continues its propagation with sub-Rayleigh speeds. For $\bar{L}_{\mathrm{h}} = 0.125$, the secondary crack accelerates to sub-Rayleigh speeds and there is no intersonic propagation beyond the patch. For $0.15 \leqslant \bar{L}_{\mathrm{h}} \leqslant 0.25$, the secondary crack accelerates after its momentary stop and briefly acquires intersonic speeds but then continues its sub-Rayleigh propagation (Fig. 11, $\bar{L}_{\mathrm{h}} = 0.2$). This seems contradictory with eventual intersonic propagation of smaller patches, for example, $\bar{L}_{\mathrm{h}} = 0.075$. Closer examination of these two cases shows that the secondary rupture accelerates faster after leaving the patch in the case of $\bar{L}_{\mathrm{h}} = 0.20$, as expected for a larger patch and hence a larger secondary crack. However, this means that the secondary crack in the case of $\bar{L}_{\mathrm{h}} = 0.20$ reaches the same locations along the interface sooner than in the case of $\bar{L}_{\mathrm{h}} = 0.075$, and hence those locations are less stressed by the advancing main crack. For $0.3 \leqslant \bar{L}_{\mathrm{h}} \leqslant 0.335$, the secondary crack transitions to intersonic speeds, reverts back to sub-Rayleigh speeds, nucleates an intersonic daughter crack in front which shortly dies, so that eventual propagation is sub-Rayleigh; such complicated behavior results from complicated dynamic stressing that combines the stress field of the main crack and the stress field released by intersonic sliding in the

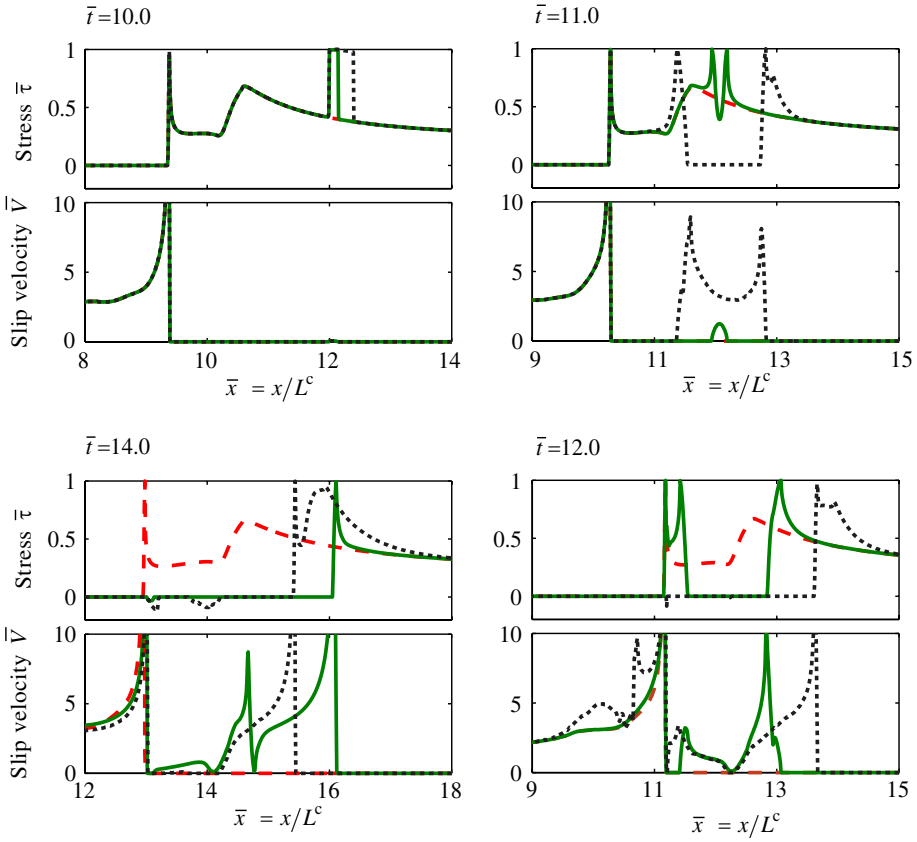

Fig. 12. Snapshots of stress and slip velocity for the cases of $\bar{L}_h = 0.075$ (solid green line) and $\bar{L}_h = 0.20$ (black dashed line with smaller dashes) with $\bar{\tau}^o = 0.25$, $\bar{\tau}^o_h = 0.85$, and more abrupt initiation of the main crack. Propagation of the main crack with no patch of higher prestress is also shown (red dashed line with larger dashes).

patch. For $0.34 \leqslant \bar{L}_h \leqslant 0.6$, the secondary crack only briefly pauses after leaving the patch, accelerating and transitioning abruptly to intersonic speeds while the main crack is still relatively far. For these larger patches, stress release during intersonic propagation within the patch must play a significant role in inducing the subsequent intersonic transition as already discussed. Fig. 11 shows the case of $\bar{L}_h = 0.34$.

This rich response is consistent with our discussion of regions of intersonic vs. sub-Rayleigh behavior in Figs. 9 and 10. Note that the illustrated case of $\bar{\tau}^o_h = 0.85$ is especially complicated since, for increasing patch size, we cross three boundaries separating regions of sub-Rayleigh and intersonic behavior (Fig. 9, top panel, $\bar{\tau}^o_h = 0.85$). The response in other cases can be much simpler, as it is, for example, in the case of $\bar{\tau}^o_h = 0.70$, where only one boundary is crossed (Fig. 9, top panel, and Fig. 11, right panel). This is because the patch prestress $\bar{\tau}^o_h = 0.70$ is relatively far from the non-dimensional static strength of 1 and hence the region "sub-Rayleigh II" does not come into play.

To illustrate the behavior of the secondary crack, we show snapshots of stress and slip rate on the interface close to the patch of higher prestress. Fig. 12 compares two cases from the left panel of Fig. 11: the case of $\bar{L}_h = 0.075$ (which results in intersonic transition) and the case of a larger patch, $\bar{L}_h = 0.20$ (for which the crack stays sub-Rayleigh). The case with no patch is also shown.

$\bar{t} = 10.0$: Stress and slip rate are the same for all three cases, with the only difference being higher stress at the location of the patch. Stress at the left corner of the patch ($\bar{x} = x/L^c = 12$) has just reached the static strength, due to the additional stress provided by the main crack. The front of the main crack is located between $\bar{x} = 9$ and 10.

$\bar{t} = 11.0$: The range of $\bar{x}$ is shifted in this snapshot. The secondary crack is still subcritical and close to the boundaries of the patch for $\bar{L}_h = 0.075$ but it is well developed and propagates outside the patch for $\bar{L}_h = 0.20$. This is not unexpected, since for $\bar{L}_h = 0.20$ the secondary crack is much larger when it exits the patch. Note that $\bar{L}^{nucl} = 0.114$.

$\bar{t} = 12.0$: The front of the secondary crack for $\bar{L}_h = 0.075$ is already intersonic (it is located close to $\bar{x} = 13$). Note that the shear stress peak of the main rupture, plotted for the case with no patch, has not yet reached this location. The secondary crack for $\bar{L}_h = 0.20$, located close to $\bar{x} = 14$, continues its sub-Rayleigh propagation and a clear shear stress peak develops in front if it.

$\bar{t} = 14.0$: The range of $\bar{x}$ is shifted in this snapshot. The intersonic secondary crack front for $\bar{L}_h = 0.075$ has passed $\bar{x} = 16$, which means that its average speed since $\bar{t} = 12.0$ has been larger than $1.5c_s$. The sub-Rayleigh front for $\bar{L}_h = 0.20$ is now behind, at about $\bar{x} = 15.5$. The shear wave peak ahead of that front has increased, almost reaching the static strength, raising the possibility of a Burridge–Andrews-type daughter crack. However, examination of further crack history (not shown) reveals that this peak starts to decrease for subsequent times and does not reach the static strength. (However, for similar situations with other parameters, a daughter crack does sometimes nucleate and either dies or leads to sustained intersonic propagation.) The tip of the main crack is at about $\bar{x} = 13$, but, at this time, all points behind the secondary crack tip have already slipped for both cases, so we have one compound rupture with the tip that coincides with the secondary crack tip.

Note that the patch makes prestress distribution on the interface discontinuous at the patch edges (Fig. 8). We have done several simulations in which prestress is smooth and differentiable between the background level $\bar{\tau}^o$ and the patch level $\bar{\tau}^o_h$. We find that simulation results with the continuous prestress distribution around the patch are very similar to those with discontinuous prestress distribution and reproduce all qualitative features, including abrupt intersonic transition and rupture behavior beyond the location of the patch.

5. Conclusions and discussion

We find that sub-Rayleigh-to-intersonic transition of mode II cracks occurs in a number of models that subject cracks to intersonic loading fields. A natural example of such stress field is stress between the shear wave peak and earliest dilatational waves propagating in front of a spontaneously expanding sub-Rayleigh mode II crack (Appendix A). If a secondary developing crack is subjected to such stress field, it can transition to intersonic speeds and maintain that intersonic propagation under a range of conditions. The Burridge–Andrews mechanism is a special case of such models. We have demonstrated sub-Rayleigh-to-intersonic transition and sustained intersonic propagation for two more models that contain "favorable heterogeneity", i.e., places susceptible to nucleation of secondary cracks. Models with a preexisting subcritical crack and with a small patch of higher prestress have been considered. Similar behavior is expected in a model with a small patch of lower static strength, and we confirm that in our simulations (not shown in this work).

In the models, a secondary crack nucleates at the location of the favorable heterogeneity and, for a range of parameters, it is driven to intersonic speeds by the advancing main crack. In models with a patch of higher prestress, interaction between the advancing stress field of the main crack and the patch results in a complicated behavior which is described in Section 4 and can be understood by considering limiting cases. We note that propagation of a secondary crack before the intersonic transition is not only nonlinear (due to friction) but also highly unsteady dynamic process and its analytical treatment, beyond qualitative arguments provided in this study, may be rather difficult. However, once crack tips become intersonic, their behavior is consistent with analytical inferences for intersonic cracks (e.g., Burridge et al., 1979; Freund, 1979; Broberg, 1994, 1995; Huang and Gao, 2001; Samudrala et al., 2002; Antipov and Willis, 2003).

In the following, we summarize and discuss other findings and their implications.

5.1. Abrupt change of crack tip speeds

In the presented models, tips of secondary cracks exhibit abrupt change of their speed from the value numerically equal to the Rayleigh wave speed c_R to an intersonic speed, and that change occurs right at the crack tip. This is different from the Burridge–Andrews mechanism, in which the daughter crack is intersonic from its very beginning. The abrupt change of a crack tip speed described in this work is an alternative way of avoiding the forbidden speed regime $[c_R, c_s]$.

Freund (1990) pointed out that, under some general assumptions, crack front speeds change in phase with applied driving stress. That implies that smooth variations in applied driving stress should result in smooth variations of the resulting crack speed. This is indeed the case in our simulations for crack speed changes within the sub-Rayleigh regime and within the intersonic regime. However, in the preexisting subcritical crack case of Section 3, all stress-related fields are continuous in time and space, but we still observe an abrupt front speed jump from speeds approaching c_R to an intersonic speed. These simulations imply that jumps from c_R to intersonic speeds may be possible, in highly unsteady situations, even if the driving stress is continuous. We emphasize that, for all cases of abrupt intersonic transition presented in this study, (i) the corresponding crack tip has been under action of an intersonic stress field of an advancing crack and, in some cases, an additional intersonic stress field radiated during intersonic sliding in the patch of higher prestress, with the latter field playing either minor or dominating role depending on the patch size, and (ii) the fronts have been highly unsteady prior to transition, rapidly accelerating from near-zero speeds to c_R.

Once the crack tip starts to propagate with intersonic speeds, the sliding process behind the tip retains larger slip velocities at the place of the old crack tip propagating with c_R and tends to create a region of decreased slip velocities propagating with c_s (which is a general feature of intersonic mode II cracks which propagate faster than shear and Rayleigh waves). This creates an impression of the old front (close to c_R) falling behind and an intersonic daughter-like crack emerging from the old front. In that sense, the abrupt transition resembles a daughter crack originating right at the secondary crack front. The region of decreased slip velocities propagating with c_s behind the intersonic crack tip tends to separate the sliding region, further reinforcing the daughter-crack analogy. (That separation also creates intersonic pulses.) Whether this is just a visual resemblance or a useful way of thinking about this transition theoretically remains a question for future study. In some cases, intersonic transition of the secondary crack beyond the patch of higher prestress is followed by transition back to sub-Rayleigh speeds. Such intersonic-to-sub-Rayleigh transition is only observed after short intersonic propagation distances, less than 1–2 L^c. When the "reverse" transition happens, the crack reverts back to the old crack front. This further supports the notion of a daughter crack originating right at the crack tip and expanding but then, in the case of the "reverse" transition, shrinking and disappearing, presumably because the intersonic loading stress due to the approaching main crack and, in some cases, due to stress waves released from the higher-stressed patch, has passed by without creating a large enough intersonic daughter crack. This consideration supports the notion of a critical crack size for intersonic transition introduced in a different context by Dunham (2006).

5.2. Prestress levels for intersonic transition and propagation

In models with favorable heterogeneities, intersonic transition and propagation can occur under much lower background prestress levels than those required by the Burridge–Andrews mechanism. This means that the level of prestress required by the Burridge–Andrews mechanism is only needed to nucleate a daughter crack on a homogeneously prestressed interface, and not to drive the daughter crack to intersonic speeds or to maintain that intersonic propagation. In Sections 3 and 4, intersonic transition and propagation occur with background prestress $\bar{\tau}^o = (\tau^o - \tau^d)/(\tau^s - \tau^d) = 0.33$, 0.25, and 0.2, while the Burridge–Andrews mechanism has critical prestress of 0.36 and needs prestress of 0.53 to achieve intersonic transition at a comparable transition length.

How low can prestress levels be and still allow intersonic transition and propagation? To investigate that question, we have considered progressively lower background prestress values $\bar{\tau}^o = 0.15$, 0.10, and 0.08 in the model with a patch of higher prestress (Section 4). Intersonic transition and sustained intersonic propagation beyond the patch occur for all these prestresses. (The other parameters of the model are: patch location $D/L^c = 12$, patch size $L_h/L^c = 0.25$, patch prestress $\bar{\tau}^o_h = 0.8$, and more abrupt initiation of the main crack.) Note that the smaller $\bar{\tau}^o$, the more challenging numerical simulations are if we would like to consider the same size of the simulated domain in terms of L^c and ensure that the cohesive zone length is adequately resolved. Combining Eqs. (1), (5), and $N^c = L^c/\Delta x$ gives the following resolution estimate: $\Lambda^o/\Delta x = (9\pi^2/32)(\bar{\tau}^o)^2 N^c$, where Λ^o is the cohesive zone length for 0^+ crack tip speeds. We use $N^c = 800$ for low prestress values which gives, for the lowest value $\bar{\tau}^o = 0.08$, $\Lambda^o/\Delta x = 14$. For sub-Rayleigh crack speeds higher than 0^+, the cohesive zone length would decrease; we verify cohesive zone resolution by plotting stress distributions on the interface

for various stages of the crack development and observing that there are several cell sizes within the cohesive zone, which means that the cohesive zone is adequately resolved (e.g., Day et al., 2005). In addition, there are virtually no cell-by-cell numerical oscillations of slip velocities behind crack tips in our simulations; such oscillations are usually a sign of inadequate numerical resolution. To the best of our knowledge, this is the first demonstration, in a simulation of spontaneous propagation of cracks, that shear cracks can propagate with intersonic speeds under such low prestress levels.

Based on our simulations, we hypothesize that, in the presence of a sufficiently large favorable heterogeneity, intersonic transition and propagation of mode II cracks are possible for any background prestress $\bar{\tau}^o > 0$ (or equivalently $\tau^o > \tau^d$). This would be analogous to sub-Rayleigh cracks, for which any background prestress τ^o higher than dynamic strength τ^d would lead to sustained crack propagation assuming that the initial crack is large enough (recall that the critical size $L^c \sim 1/(\tau^o - \tau^d)^2$ and L^c increases rapidly as τ^o approaches τ^d).

5.3. Transition distance

Models with favorable heterogeneities have transition distances that depend on the position of heterogeneity. Transition lengths determined by Andrews (1976) for homogeneous stress and strength provide an upper bound for transition lengths in models considered here.

Andrews (1976) numerically showed that non-dimensional transition distance L_{BA}/L^c on a homogeneously prestressed interface, with initial conditions appropriate for a quasi-static critical crack, is a function of the seismic ratio S (or, equivalently, prestress $\bar{\tau}^o$). For high enough prestress (i.e., $S < S_{crit}$), transition length L_{BA}/L^c of the Burridge–Andrews mechanism is determined by the position where the maximum of the shear stress peak reaches static strength. For smaller prestress (i.e., $S \geqslant S_{crit}$), no intersonic transition is possible by the Burridge–Andrews mechanism, and L_{BA}/L^c is infinity. This study shows that if favorable heterogeneity is located closer to the main crack initiation region than L_{BA}/L^c, then intersonic transition may occur due to the heterogeneity, with the transition length approximately given by the location of the heterogeneity. For example, all models with sustained intersonic propagation in Sections 3 and 4 have transition lengths dictated by the location of heterogeneity $D/L^c = 12$. If heterogeneities were not present in the models, transition lengths by the Burridge–Andrews mechanism would be infinite for the prestress values studied.

5.4. Importance of crack initiation procedure

The procedure of main crack initiation significantly affects subsequent crack propagation and hence the loading provided by the main crack to the location of favorable heterogeneity. That, in turn, affects the crack tip speed beyond the location of heterogeneity (Section 4, Fig. 9 vs. Fig. 10).

In the smooth initiation procedure (described in Section 3), we stop the time-dependent loading increase when the initial half size L_{ini} of the main crack reaches the nucleation half size L^{nucl} determined by Uenishi and Rice (2003). That plus the slow loading we choose ensures that the initiation procedure mimics tectonically driven slow nucleation on faults in the Earth's crust. Our more abrupt crack initiation (Section 4) initiates the main crack by imposing prestress 1% larger than static strength over length $2L^c$, a procedure typical in modeling single earthquakes. For the background prestress levels used in this study, $2L^c$ is appreciably larger than $2L^{nucl}$ (Table 1). That creates larger initial crack sizes and faster acceleration of the main crack, by overstressing the main crack initially in comparison with a slow, quasi-static nucleation process. The resulting higher shear stresses ahead of the main crack promote intersonic transition. This more abrupt initiation procedure can be considered a proxy for larger propagation distances as explained in Section 4.

Note that similar overstressing of the crack can be achieved with our smooth initiation procedure by using faster time-dependent loading and continuing it until initial crack half sizes larger than L^{nucl} would be created. Under slow tectonic loading characteristic for earthquakes, nucleation zones should become unstable after reaching half lengths of L^{nucl}, as shown by Uenishi and Rice (2003) and confirmed in this work, making subsequent tectonic loading irrelevant on the time scale of the dynamic event. Hence nucleation half sizes larger than L^{nucl} are hard to obtain under slowly increasing loading. In a model, any loading added to the nucleation zone after a developing nucleation site reaches the half size L^{nucl} represents extra loading or

overstressing. More abrupt initiation procedure similarly provides the crack with extra loading. It is possible that such extra loading can result on real faults for some dynamic triggering scenarios or rapid strength variations. However, it is important to keep in mind that nucleation procedures that are abrupt and/or overstress the crack initially may not be the most common ones on tectonically loaded faults.

In Sections 3 and 4, we have considered relatively low background prestress levels, lower than the ones needed for intersonic transition by the Burridge–Andrews mechanism. We have conducted additional simulations that use the more abrupt initiation procedure with higher prestress levels in the absence of heterogeneities. In those simulations, the main crack achieves intersonic speeds much sooner than predicted by the Burridge–Andrews mechanism. If we load the nucleation region even more, we can make the main crack transition to intersonic speeds right outside the nucleation zone. In those cases, transition to intersonic speeds happens by either the abrupt transition mechanism described in this work, or by the Burridge–Andrews daughter mechanism, or both (that is, in some cases, the crack experiences abrupt speed changes twice, once by the abrupt mechanism described in this study, and the second time by nucleating an intersonic Burridge–Andrews daughter crack in front of the already intersonic crack).

These results for overstressed cracks are consistent with the studies of Festa and Vilotte (2006) and Shi et al. (2007) who considered, in the absence of stress heterogeneity beyond the nucleation region, the dependence of intersonic transition and rupture mode on the initiation procedure, and with the study of Geubelle and Kubair (2001) and Shi and Ben-Zion (2006). In Shi et al. (2007), the initiation procedure is similar to the more abrupt procedure of this work, in that a value of shear stress about 3% above the static strength is used over a zone which is about 3–6 times larger than $2L^{\text{nucl}}$. That may explain the rapid transition of rupture to intersonic speeds in the model of Shi et al. (2007) for high background prestress levels. (Note that their study uses a friction law of a rate and state type.) In Festa and Vilotte (2006), a nucleation procedure with a peaked stress in the nucleation zone is used. They find that intersonic transition is enhanced, and transition distances are shorter, when peaked loading with widths progressively larger than $2L^{\text{nucl}}$ is used. Geubelle and Kubair (2001), while concentrating on mixed-mode failure, considered, in part, intersonic transition for a purely mode II crack. They found that the crack transitions to intersonic speeds by abruptly changing the speed of its tip at distances very close to the crack initiation zone. The initiation procedure in Geubelle and Kubair (2001) was not described in detail but short transition distances obtained in that work suggest that the initiation procedure provided some overstressing, in the sense defined above.

5.5. Propagation speeds in the intersonic regime

Once a crack acquires intersonic speeds, it tends to accelerate, in our models, to speeds larger than $\sqrt{2}c_s$ and close to the dilatational wave speed c_p. This is consistent with the theoretical study of Burridge et al. (1979) who concluded that intersonic ruptures in models with finite tractions, constant fracture energy, and homogeneous prestress would accelerate to c_p (our models have homogeneous prestress after the location of favorable heterogeneity). This result is also consistent with experiments (e.g., Xia et al., 2004). Samudrala et al. (2002) found that, for velocity-weakening interfaces, the open interval of speeds from $\sqrt{2}c_s$ to c_p corresponds to stable rupture growth, so speeds larger than $\sqrt{2}c_s$ should be typical for velocity-weakening interfaces as well. Note that, for singular cracks, $\sqrt{2}c_s$ is the only possible intersonic speed, as this is the only speed at which the energy release rate is positive (Freund, 1990), but that is no longer the case for cohesive-zone models with finite tractions.

5.6. Implications for earthquake dynamics

Models for intersonic transition and propagation proposed here may have important consequences for earthquake dynamics. Favorable heterogeneities considered in this work are likely to be present on real faults. Earthquake models predict that seismic events are preceded by quasi-static slip in so-called nucleation zones (e.g., Lapusta et al., 2000; Lapusta and Rice, 2003) that are analogous to preexisting subcritical cracks considered in Section 3. Faults are likely to harbor multiple nucleation zones. When one of these zones gives rise to an earthquake, the other developing nucleation zones would find themselves under the stress field of an approaching dynamic crack, creating the scenario considered in Section 3. How heterogeneous stress and

strength are on faults and on what scales is an active area of current research. Seismic inversions typically contain regions of high and low slip, which likely indicate variations in fault prestress and/or strength. In particular, faults may contain patches of higher prestress considered in Section 4 or patches of lower strength. We do not present results for patches of lower strength in this work but our simulations show that they are similar to results for patches of higher prestress.

Our modeling indicates that intersonic transition may be dominated by those heterogeneities. In that case, interpretation of inferred intersonic propagation using the Burridge–Andrews mechanism for homogeneous prestress and strength could lead to misleading constraints on background prestress levels or friction properties.

Note that even when sustained intersonic propagation does not occur in our models, the presence of favorable heterogeneity often mimics intersonic propagation locally by producing significant advance in the crack tip location. For a preexisting subcritical crack or a patch of sufficiently high prestress (higher than α defined in Section 4), the tip of combined rupture propagating beyond the patch is that of the secondary crack for patches close to and larger than L^{nucl} (for smaller patches, the secondary crack is overtaken by the main crack). Even if the secondary crack is sub-Rayleigh, average rupture speed would appear to be intersonic in the region that surrounds the patch. Consider, for example, the case with a patch of the size $L_{\mathrm{h}}/L^{\mathrm{c}} = 0.20$ from the left panel of Fig. 11. Eventual propagation is sub-Rayleigh in that case, but the secondary crack tip is about $2L^{\mathrm{c}}$ ahead of where the main crack front would have been if there were no patch. Hence the average crack speed in the space interval shown in Fig. 11 (from $\bar{x} = 9$ to 16) is $1.4c_{\mathrm{s}}$. In addition, favorable heterogeneity provides the main crack with additional stress release which temporarily increases stresses in front of the crack. That makes intersonic transition due to another heterogeneity or due to the Burridge–Andrews mechanism more likely.

There are a number of ways in which the presented conceptual models could be extended to make them more directly relevant to earthquake phenomena.

(i) This study uses linear slip-weakening friction which has constant fracture energy and governs both initiation of cracks and their dynamic propagation. It becomes increasingly clear that fault behavior during earthquakes is much more complex. Nucleation processes are likely governed by rate and state friction laws which have characteristic nucleation lengths of order meters (e.g., Lapusta and Rice, 2003, and references therein) although larger nucleation zones may result due to low effective normal stresses or friction properties close to rate-neutral. Dynamic propagation is likely to activate a number of additional weakening mechanisms, some of them related to shear heating, which could lead either to a combined slip- and rate-weakening law or to nonlinear slip-weakening behavior with larger fracture energies for larger slips (e.g., Rice, 2006). In addition, off-fault bulk dissipation could have a significant effect on rupture dynamics and may delay intersonic transition (Templeton and Rice, 2006); that effect may be possible to approximately represent by appropriate variations in fracture energy (Andrews, 2005). Seismic observations and current theories indicate that, during dynamic propagation, characteristic crack lengths could be significantly larger than nucleation lengths. Hence it is important to study rupture interaction with heterogeneities on interfaces governed by nonlinear slip-weakening laws and also by combined laws that incorporate rate and state laws at slow slip velocities and nonlinear slip-weakening laws at higher, seismic slip velocities.

(ii) This study considers 2D models of in-plane sliding. Large strike-slip earthquakes occur on faults that have long strike lengths (hundreds of km) but limited depth extent (15–20 km or so). Hence their dynamics, while dominated by in-plane sliding, is also influenced by 3D aspects, especially the finite fault width, which have been shown to have adverse effects on intersonic transition (e.g., Day, 1982a,b; Fukuyama and Olsen, 2002; Dunham, 2006). This means that transition models presented in this 2D study would need to employ larger heterogeneities and/or larger background prestress in 3D. We plan to extend this study to 3D, using parameters informed by our 2D results. Note that most 3D studies of intersonic transition used models without a free surface. A free surface would favor intersonic transition (e.g., Dunham and Archuleta, 2004; Kaneko et al., 2006).

(iii) Pulse-like rupture propagation on real faults may be more common than crack-like rupture propagation (e.g., Das and Kostrov, 1988; Heaton, 1990; Zheng and Rice, 1998; Nielsen et al., 2000; Ben-Zion, 2001;

Shi et al., 2007). Hence it would be important to consider the potential intersonic transition due to preexisting heterogeneity for the case of pulse-like main rupture. Such main rupture can be created by switching to more realistic friction laws discussed above. Note that recent laboratory experiments have demonstrated intersonic transition of pulse-like ruptures (Lu et al., 2006).

(iv) Stress and strength distributions on faults in the Earth's crust can be much more complicated than assumed in this study. Certain types of heterogeneous stress distributions result in slower rupture speeds than the speeds that would correspond to mean values of stress (e.g., Day, 1982b). While one can assume any prestress distribution for a simulation of one instance of dynamic rupture, stress distribution on faults before a large earthquake is the result of a complicated history of seismic and aseismic sliding. That history would tend to redistribute stress and may exclude some prestress distributions before a large earthquake and hence certain rupture behaviors (Lapusta and Liu, 2006). Hence it is important to simulate long deformation histories of faults, to be able to study simulated earthquakes under prestress distributions that naturally arise as the result of prior sliding history (Lapusta et al., 2000; Lapusta and Rice, 2003; Lapusta and Liu, 2006).

In a broader context, this study shows the importance of incorporating heterogeneities into models of rupture dynamics. This study indicates that a small preexisting crack or higher-stressed patch can completely change the failure process on the interface, perturbing a sub-Rayleigh crack into becoming intersonic. This emphasizes the need to systematically study effects of stress and strength heterogeneities on rupture behavior.

Acknowledgments

This research was supported by the National Science Foundation and by the Southern California Earthquake Center. SCEC is funded by NSF Cooperative Agreement EAR-0106924 and USGS Cooperative Agreement 02HQAG0008. The SCEC contribution number for this paper is 1090. The numerical simulations for this research were performed on Caltech Division of Geological and Planetary Sciences Dell cluster. We thank Yehuda Ben-Zion and an anonymous reviewer for helpful comments.

Appendix A. Intersonic loading field due to an accelerating sub-Rayleigh mode II crack

For a sufficiently smooth dynamic shear stress field $\tau(x,t)$, let us define its propagation speed $c(x,t)$ as

$$c(x,t) = -\frac{\partial\tau(x,t)/\partial t}{\partial\tau(x,t)/\partial x}. \tag{A.1}$$

A stress field with $c(x,t) > c_s$ and $\partial\tau(x,t)/\partial t > 0$ represents stress increase that travels along the interface with an intersonic speed. We call such stress fields "intersonic loading fields" in this study. Intersonic loading fields should promote failure of the interface with intersonic speeds (and they indeed do as this study demonstrates). Simulations show that a sub-Rayleigh mode II crack spontaneously accelerating on a uniformly prestressed interface governed by linear slip-weakening friction develops a shear stress peak ahead of its tip (e.g., Andrews, 1976, Figs. 2 and 3), and stress in front of the peak represents an intersonic loading field.

This can be theoretically understood by considering a self-similar singular crack model, in which the stress field takes a general form of $\tau(x,t) = \tilde{\tau}(x/t)$. If a self-similar crack expands bilaterally with rupture speed $v_r < c_R$ under uniform prestress τ^o on an interface with dynamic resistance τ^d, the stress field ahead of the crack between the dilatational and shear wave fronts can be expressed as (e.g., Burridge, 1973; Freund, 1990):

$$\tau(x,t) = \tilde{\tau}(c = x/t) = \tau^o + (\tau^o - \tau^d)\frac{F(h,\omega)}{I(h)}, \tag{A.2}$$

$$h = 1/v_r, \quad a = 1/c_p, \quad b = 1/c_s, \quad \omega = t/x = 1/c, \tag{A.3}$$

$$F(h,\omega) = \int_a^\omega \frac{4\xi^2\sqrt{\xi^2 - a^2}}{(h^2 - \xi^2)^{3/2}\sqrt{b^2 - \xi^2}}\,\mathrm{d}\xi, \tag{A.4}$$

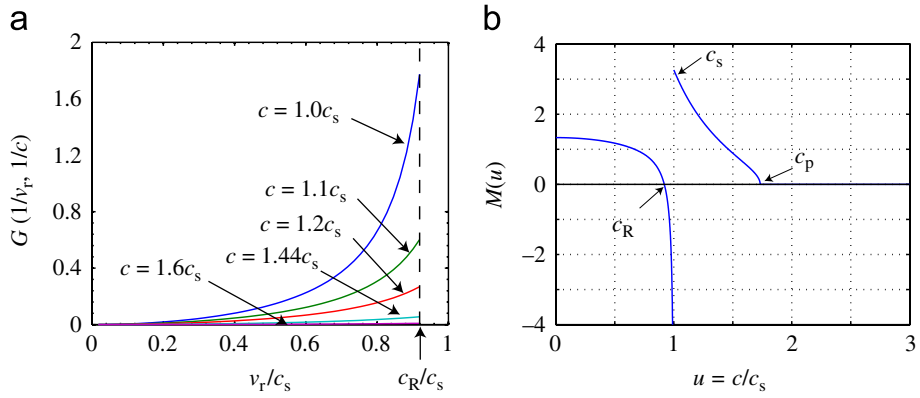

Fig. A.1. (a) $G(1/v_r, 1/c) = (\tilde{\tau}(c) - \tau^o)/(\tau^o - \tau^d)$ for different $c > c_s$ and rupture speed v_r. (b) Mode II kernel $M(u)$ of the space–time representation of $f(x,t)$.

$$I(h) = \int_0^\infty \frac{(b^2 + 2\xi^2)^2 - 4\xi^2\sqrt{a^2+\xi^2}\sqrt{b^2+\xi^2}}{(h^2+\xi^2)^{3/2}\sqrt{b^2+\xi^2}}\,\mathrm{d}\xi. \tag{A.5}$$

The propagation speed of a self-similar stress field $\tau(x,t)$ is $c(x,t) = x/t$. For points located between the dilatational and shear wave fronts $c_s < x/t < c_p$, stress propagates with intersonic speeds and increases if $v_r < c_R$:

$$\frac{\partial\tau}{\partial t} = (\tau^o - \tau^d)\frac{\partial F}{\partial\omega}\frac{\partial\omega}{\partial t} = \frac{\tau^o - \tau^d}{x}\frac{4\omega^2\sqrt{\omega^2 - a^2}}{(h^2-\omega^2)^{3/2}\sqrt{b^2-\omega^2}} > 0. \tag{A.6}$$

Therefore, the stress field between the dilatational and shear wave fronts of a sub-Rayleigh self-similar crack represents an intersonic loading field.

Larger sub-Rayleigh crack front speeds v_r correspond to larger stress between the dilatational and shear wave fronts. To show that, let us define $G(1/v_r, 1/c) = (\tilde{\tau}(c) - \tau^o)/(\tau^o - \tau^d)$, hence $G(h,\omega) = F(h,\omega)/I(h)$, and

$$\frac{\partial G(h,\omega)}{\partial h} = \frac{I(h)\partial F(h,\omega)/\partial h - F(h,\omega)\partial I(h)/\partial h}{I^2(h)} = \frac{\frac{\partial F}{\partial h}/F - \frac{\partial I}{\partial h}/I}{FI^3}. \tag{A.7}$$

Notice that $F(h = 1/v_r, \omega = 1/c) > 0$ and $I(h = 1/v_r) > 0$ for any $0 < v_r < c_R$ and $c_s \leqslant c < c_p$, and

$$\frac{\partial F}{\partial h} = -\frac{3}{h}\int_a^\omega \frac{h^2}{h^2-\xi^2}\frac{4\xi^2\sqrt{\xi^2-a^2}}{(h^2-\xi^2)^{3/2}\sqrt{b^2-\xi^2}}\,\mathrm{d}\xi < -\frac{3}{h}F, \tag{A.8}$$

$$\frac{\partial I}{\partial h} = -\frac{3}{h}\int_0^\infty \frac{h^2}{h^2+\xi^2}\frac{(b^2+2\xi^2)^2 - 4\xi^2\sqrt{a^2+\xi^2}\sqrt{b^2+\xi^2}}{(h^2+\xi^2)^{3/2}\sqrt{b^2+\xi^2}}\,\mathrm{d}\xi > -\frac{3}{h}I. \tag{A.9}$$

Combining Eqs. (A.7)–(A.9), we get

$$\frac{\partial G(h,\omega)}{\partial h} < 0; \quad h = 1/v_r > 1/c_R \quad \text{and} \quad 1/c_p \leqslant \omega < 1/c_s. \tag{A.10}$$

One can also find that $G(1/v_r, 1/c_s) \to 1.775$ as $v_r \to c_R$, as shown in Fig. A.1a, which is consistent with the value of S_{crit} computed by Andrews (1976).

The theoretical considerations above are based on a self-similar crack model, in which stress is inverse square-root singular at the rupture tip for sub-Rayleigh propagation. However, as Andrews (1976) pointed out, a crack governed by a linear slip-weakening law can be well approximated by the self-similar solution after it propagates through several critical lengths L^c.

Appendix B. Expressions for stress transfer functional in the spectral boundary integral method

In simulations, we use a spectral boundary integral method (Section 2), in which Fourier coefficients of the stress transfer functional $f(x,t)$ are related to Fourier coefficients of slip $\delta(x,t)$ and its history (Perrin et al., 1995; Geubelle and Rice, 1995; Lapusta et al., 2000). The simulated domain of length L is discretized into N elements and we write

$$\delta(x,t) = \sum_{k=-N/2}^{N/2} \hat{\delta}(k,t)\exp(\mathrm{i}2\pi kx/L), \tag{B.1}$$

$$f(x,t) = \sum_{k=-N/2}^{N/2} \hat{f}(k,t)\exp(\mathrm{i}2\pi kx/L). \tag{B.2}$$

The Fourier coefficients $\hat{f}(k,t)$ and $\hat{\delta}(k,t)$ are related by

$$\hat{f}(k,t) = -\frac{\mu\tilde{k}}{2}\int_0^t C_{\mathrm{II}}(\tilde{k}c_s t')\hat{\delta}(k,t-t')\tilde{k}c_s\,\mathrm{d}t', \tag{B.3}$$

$$C_{\mathrm{II}}(T) = J_1(T)/T + 4T[W(c_pT/c_s) - W(T)] - 4\frac{c_p}{c_s}J_0(c_pT/c_s) + 3J_0(T), \tag{B.4}$$

where $\tilde{k} = 2\pi k/L$, $C_{\mathrm{II}}(T)$ is the mode II convolution kernel (Geubelle and Rice, 1995), $J_0(T)$ and $J_1(T)$ are Bessel functions, and

$$W(T) = 1 - \int_0^T \frac{J_1(x)}{x}\,\mathrm{d}x. \tag{B.5}$$

Integration of Eq. (B.3) by parts separates the stress functional into static (long-term) and transient dynamic parts:

$$\hat{f}(k,t) = -\mu\tilde{k}\left(1 - \frac{c_s^2}{c_p^2}\right)\hat{\delta}(k,t) + \frac{\mu\tilde{k}}{2}\int_0^t K_{\mathrm{II}}(\tilde{k}c_s t')\frac{\partial\hat{\delta}(k,t-t')}{\partial t}\,\mathrm{d}t', \tag{B.6}$$

$$K_{\mathrm{II}}(T) = \int_T^\infty C_{\mathrm{II}}(\eta)\,\mathrm{d}\eta = 2\left(1 - \frac{c_p^2}{c_s^2}\right) - \int_0^T C_{\mathrm{II}}(\eta)\,\mathrm{d}\eta. \tag{B.7}$$

The integral term on the right-hand side of Eq. (B.6) describes dynamic stress changes due to waves. If it is neglected, the resulting formulation is referred to as "quasi-dynamic". The quasi-dynamic formulation differs from the quasi-static formulation in that it contains the radiation damping term, $\mu V/(2c_s)$, which captures some dynamic effects. The quasi-dynamic formulation is widely used in earthquake studies to simplify computations. We use the quasi-dynamic formulation during slow and relatively long smooth initiation phases discussed in Section 3, to speed up computations and to ensure that no stress waves from the initiation procedure exist in the model at later times. After the initiation phase, we use fully dynamic formulation. Note that kernel $C_{\mathrm{II}}(T)$ oscillates with decaying amplitude which allows to truncate the integral term (e.g., Lapusta et al., 2000; Day et al., 2005). However, in this study we do not employ any truncation, to compute dynamic stress fields as accurately as possible.

Appendix C. Some aspects of crack tip behavior during abrupt intersonic transition

As we show in Sections 3 and 4, if a secondary crack finds itself under the action of an intersonic loading field generated by an approaching main crack, the tip of the secondary crack can rapidly accelerate to values numerically indistinguishable from c_R and then abruptly jump to an intersonic speed. While steady crack propagation with c_R would result in zero cohesive zone length and infinite slip velocities and hence it is impossible, our simulations show that transient propagation with c_R may be possible. The crack tip jumps to

an intersonic speed by initiating sliding just one cell Δx away from the crack tip (Figs. 6 and 7). At that moment, shear stress in the cell immediately in front of the tip is below static strength, and shear stress in the next cell has reached static strength (Fig. 7). The same process is observed for smaller and smaller Δx, with the shear stress in the intermediate cell closer and closer to static strength. Hence, in the limit $\Delta x \to 0$, we expect intersonic transition to occur right at the crack tip.

To understand why shear stress is lower immediately next to the crack tip than farther ahead, let us consider a mode II crack tip that has propagated (for a short time) with the Rayleigh wave speed c_R. How does the wave radiation from that tip at time t_0 influence the stress field in front of the tip at the time $t > t_0$? To answer that question, let us consider the stress transfer functional $f(x,t)$ (Eq. (3)) in the space–time domain (e.g., Cochard and Rice, 1997):

$$f(x,t) = \frac{\mu c_s}{2\pi} \int_{-\infty}^{t} \int_{-\infty}^{+\infty} M\left(\frac{x-\zeta}{c_s(t-\theta)}\right) \frac{\delta_{,\zeta\zeta}(\zeta,\theta)}{c_s(t-\theta)}\, d\zeta\, d\theta, \tag{C.1}$$

$$M(u) = \begin{cases} \dfrac{4\sqrt{1-u^2}\sqrt{1-(c_s^2/c_p^2)u^2} - (2-u^2)^2}{u^2\sqrt{1-u^2}} & \text{if } |u|<1, \\ \dfrac{4\sqrt{1-(c_s^2/c_p^2)u^2}}{u^2} & \text{if } 1<|u|<c_p/c_s, \\ 0 & \text{if } |u|>c_p/c_s. \end{cases} \tag{C.2}$$

The integral kernel $M(u)$ is plotted in Fig. A.1b. Note that $M(u)<0$ for $c_R/c_s<u<1$. Let us denote the location of the crack tip at the time t by $x_r(t)$, where $x_r(t) = x_r(t_0) + c_R(t-t_0)$.

Numerical calculation approximates the above integral with discretized space and time, effectively assuming constant $\delta_{,\zeta\zeta}$ within the cell size Δx and time step Δt. Therefore rupture tip located at $x_r(t_0)$ at the time t_0 contributes to the stress functional $f(x,t)$ by an amount $\Delta f(x_r(t_0),t_0)$:

$$\Delta f(x_r(t_0),t_0) = \frac{\mu c_s}{2\pi} M\left(\frac{x-x_r(t_0)}{c_s(t-t_0)}\right) \frac{\delta_{,\zeta\zeta}(x_r(t_0),t_0)}{c_s(t-t_0)} \Delta t\, \Delta x. \tag{C.3}$$

In Eq. (C.3), $\delta_{,\zeta\zeta}(x_r(t_0),t_0)$ is the value for the spatial cell located in the ruptured region ($x<x_r(t_0)$) and, for sufficiently small cell size, its sign can be obtained by considering $\zeta \to x_r^-(t_0)$. Since $\delta(\zeta \geqslant x_r(t_0),t_0) = 0$ and $\delta_{,\zeta}(x_r^-(t_0),t_0) = \delta_{,\zeta}(x_r^+(t_0),t_0) = 2\varepsilon_{xx}(x_r(t_0),t_0)) = 0$, where ε_{xx} is the normal strain in x direction, we find

$$0<\delta(\zeta<x_r(t_0),t_0) = \tfrac{1}{2}\delta_{,\zeta\zeta}(x_r^-(t_0),t_0)(\zeta - x_r(t_0))^2 + o((\zeta - x_r(t_0))^2), \tag{C.4}$$

and hence $\delta_{,\zeta\zeta}(x_r^-(t_0),t_0)>0$. From properties of kernel M and Eqs. (C.3) and (C.4), we obtain for $t>t_0$:

$$\begin{cases} \Delta f(x_r(t_0),t_0)<0, & x_r(t_0)+c_R(t-t_0)<x<x_r(t_0)+c_s(t-t_0), \\ \Delta f(x_r(t_0),t_0)>0, & x_r(t_0)+c_s(t-t_0)<x<x_r(t_0)+c_p(t-t_0). \end{cases} \tag{C.5}$$

At time t, the crack tip is at $x_r(t) = x_r(t_0) + c_R(t-t_0)$. Therefore $\Delta f(x_r(t_0),t_0)<0$ for $x \in [x_r(t), x_r(t) + (c_s - c_R)(t-t_0)]$, and $\Delta f(x_r(t_0),t_0)>0$ for $x \in [x_r(t) + (c_s - c_R)(t-t_0), x_r(t) + (c_p - c_R)(t-t_0)]$. This means that the crack tip traveling with c_R at time t_0 contributes negatively to shear stress at the part of the interface immediately in front of the current rupture tip (at time t) and positively to shear stress a little farther ahead. This relation holds for all times $t_0<t$ for which the crack has propagated with a speed at or close to c_R. Piling up of these contribution from different $t_0<t$ may explain the observed stress distribution during intersonic transition in our simulations (Fig. 7), where shear stress is lower in the cell immediately in front of the crack tip and reaches static strength in the next cell. In the continuum solution, the negative contribution of the crack tip to location immediately ahead may be exactly balanced by contributions from other parts of the crack, as our simulations suggest for decreasing cell sizes. But in a discretized calculation, contributions from the crack front are evidently overemphasized, which is not surprising since one would expect largest numerical errors to come from crack tips where slip velocity and stress vary rapidly.

References

Adams, G.G., 2001. An intersonic slip pulse at a frictional interface between dissimilar materials. J. Appl. Mech. 68 (1), 81–86.

Andrews, D.J., 1976. Rupture velocity of plane strain shear cracks. J. Geophys. Res. 81, 5679–5687.

Andrews, D.J., 2005. Rupture dynamics with energy loss outside the slip zone. J. Geophys. Res. 110, B01307.

Antipov, Y.A., Willis, J.R., 2003. Transient loading of a rapidly advancing Mode-II crack in a viscoelastic medium. Mech. Mater. 35, 415–431.

Archuleta, R.J., 1984. A faulting model for the 1979 Imperial Valley earthquake. J. Geophys. Res. 89 (B6), 4559–4585.

Ben-Zion, Y., 2001. Dynamic ruptures in recent models of earthquake faults. J. Mech. Phys. Solids 49, 2209–2244.

Bernard, P., Baumont, D., 2005. Shear Mach wave characterization for kinematic fault rupture models with constant supershear rupture velocity. Geophys. J. Int. 162 (2), 431–447.

Bhat, H.S., Dmowska, R., King, G.C.P., Klinger, Y., Rice, J.R., 2007. Off-fault damage patterns due to supershear ruptures with application to the 2001 Mw 8.1 Kokoxili (Kunlun) Tibet earthquake. J. Geophys. Res. 112, B06301.

Bouchon, M., Vallée, M., 2003. Observation of long supershear rupture during the magnitude 8.1 Kunlunshan earthquake. Science 301, 824–826.

Bouchon, M., Bouin, M.P., Karabulut, H., Toksöz, M.N., Dietrich, M., Rosakis, A.J., 2001. How fast is rupture during an earthquake? New insights from the 1999 Turkey earthquakes. Geophys. Res. Lett. 28 (14), 2723–2726.

Broberg, K.B., 1994. Intersonic bilateral slip. Geophys. J. Int. 119, 706–714.

Broberg, K.B., 1995. Intersonic mode II crack expansion. Arch. Mech. 47, 859–871.

Burridge, R., 1973. Admissible speeds for plane-strain self-similar shear cracks with friction but lacking cohesion. Geophys. J. Int. 35 (4), 439–455.

Burridge, R., Conn, G., Freund, L.B., 1979. The stability of a rapid mode II shear crack with finite cohesive traction. J. Geophys. Res. 85 (B5), 2210–2222.

Cochard, A., Rice, J.R., 1997. A spectral method for numerical elastodynamic fracture analysis without spatial replication of the rupture event. J. Mech. Phys. Solids 45, 1393–1418.

Cochard, A., Rice, J.R., 2000. Fault rupture between dissimilar materials: ill-posedness, regularization, and slip–pulse response. J. Geophys. Res. 105 (B11), 25891–25907.

Das, S., Kostrov, B.V., 1988. An investigation of the complexity of the earthquake source time function using dynamic faulting models. J. Geophys. Res. 93, 8035–8050.

Day, S.M., 1982a. Three-dimensional finite difference simulations of fault dynamics: rectangular faults with fixed rupture velocity. Bull. Seismol. Soc. Am. 72, 705–727.

Day, S.M., 1982b. Three-dimensional simulations of spontaneous rupture: the effect of nonuniform prestress. Bull. Seismol. Soc. Am. 72, 1881–1902.

Day, S.M., Dalguer, L.A., Lapusta, N., Liu, Y., 2005. Comparison of finite difference and boundary integral solutions to three-dimensional spontaneous rupture. J. Geophys. Res. 110, B12307.

Dunham, M., 2006. Conditions governing the occurrence of supershear ruptures under slip-weakening friction. J. Geophys. Res. 112, B07302.

Dunham, E.M., Archuleta, R.J., 2004. Evidence for a supershear transition during the 2002 Denali fault earthquake. Bull. Seismol. Soc. Am. 94, 256–268.

Dunham, E.M., Archuleta, R.J., 2005. Near-source ground motion from steady state dynamic rupture pulses. J. Geophys. Res. 32, L03302.

Dunham, E.M., Favreau, P., Carlson, J.M., 2003. A supershear transition mechanism for cracks. Science 299, 1557–1559.

Ellsworth, W.L., Celebi, M., Evans, J.R., Jensen, E.G., Kayen, R., Metz, M.C., Nyman, D.J., Roddick, J.W., Spudich, P., Stephens, C.D., 2004. Near-field ground motion of the 2002 Denali fault, Alaska, earthquake recorded at Pump Station 10. Earthquake Spectra 20 (3), 597–615.

Festa, G., Vilotte, J.P., 2006. Influence of the rupture initiation on the intersonic transition: crack-like versus pulse-like modes. Geophys. Res. Lett. 33 (15), L15320.

Freund, L.B., 1979. The mechanics of dynamic shear crack propagation. J. Geophys. Res. 84, 2199–2209.

Freund, L.B., 1990. Dynamic Fracture Mechanics. Cambridge University Press, New York.

Fukuyama, E., Olsen, K.B., 2002. A condition for super-shear rupture propagation in a heterogeneous stress field. Pure. Appl. Geophys. 157, 2047–2056.

Gao, H., Huang, Y., Abraham, F.F., 2001. Continuum and atomistic studies of intersonic crack propagation. J. Mech. Phys. Solids 49, 2113–2132.

Geubelle, P.H., Rice, J.R., 1995. A spectral method for 3D elastodynamic fracture problems. J. Mech. Phys. Solids 43, 1791–1824.

Geubelle, P.H., Kubair, D.V., 2001. Intersonic crack propagation in homogeneous media under shear-dominated loading: numerical analysis. J. Mech. Phys. Solids 49 (3), 571–587.

Harris, R.A., Day, S.M., 1997. Effects of a low-velocity zone on a dynamic rupture. Bull. Seismol. Soc. Am. 87 (5), 1267–1280.

Heaton, T.H., 1990. Evidence for and implications of self-healing pulses of slip in earthquake rupture. Phys. Earth Planet. Inter. 64, 1–20.

Huang, Y., Gao, H., 2001. Intersonic crack propagation—Part I: the fundamental solution. J. Appl. Mech. 68 (2), 169–175.

Kaneko, Y., Lapusta, N., Ampuero, J., 2006. Spectral element modeling of earthquake nucleation and spontaneous rupture on rate and state faults. Eos Trans. AGU 87(52) (Fall Meet. Suppl.), S52B-06.

Lapusta, N., Liu, Y., 2006. Three-dimensional elastodynamic simulations of seismic and aseismic slip history of a planar strike-slip fault. Eos Trans. AGU 87 (52) (Fall Meet. Suppl.) Abstract S34A-07.

Lapusta, N., Rice, J.R., 2003. Nucleation and early seismic propagation of small and large events in a crustal earthquake model. J. Geophys. Res. 108 (B4), 2205.

Lapusta, N., Rice, J.R., Ben-Zion, Y., Zheng, G., 2000. Elastodynamic analysis for slow tectonic loading with spontaneous rupture episodes on faults with rate- and state-dependent friction. J. Geophys. Res. 105, 23765–23789.

Lu, X., Lapusta, N., Rosakis, A.J., 2006. Constraining friction laws by experimental observations and numerical simulations of various rupture modes. Eos Trans. AGU 87(52) (Fall Meet. Suppl.) S33C-04.

Madariaga, R., Olsen, K.B., 2000. Criticality of rupture dynamics in 3D. Pure Appl. Geophys. 157, 1981–2001.

Needleman, A., Rosakis, A.J., 1999. The effect of bond strength and loading rate on the conditions governing the attainment of intersonic crack growth along interfaces. J. Mech. Phys. Solids 47, 2411–2449.

Nielsen, S.B., Carlson, J.M., Olsen, K.B., 2000. Influence of friction and fault geometry on earthquake rupture. J. Geophys. Res. 105, 6069–6088.

Olsen, K.B., Madariaga, R., Archuleta, R.J., 1997. Three-dimensional dynamic simulation of the 1992 Landers earthquake. Science 278, 834–838.

Palmer, A.C., Rice, J.R., 1973. The growth of slip surfaces in the progressive failure of overconsolidated clay slopes. Proc. R. Soc. London Ser. A 332, 527–548.

Perrin, G., Rice, J.R., Zheng, G., 1995. Self-healing slip pulse on a frictional surface. J. Mech. Phys. Solids 43, 1461–1495.

Ranjith, K., Rice, J.R., 2001. Slip dynamics at an interface between dissimilar materials. J. Mech. Phys. Solids 49 (2), 341–361.

Rice, J.R., 1980. The mechanics of earthquake rupture. In: Dziewonski, A.M., Boschi, E. (Eds.), Physics of the Earth's Interior. Proceedings of the International School of Physics Enrico Fermi, Course 78. Elsevier, New York, pp. 555–649.

Rice, J.R., 2006. Heating and weakening of faults during earthquake slip. J. Geophys. Res. 111, B05311.

Rosakis, A.J., 2002. Intersonic shear cracks and fault ruptures. Adv. Phys. 51 (4), 1189–1257.

Rosakis, A.J., Samudrada, O., Coker, D., 1999. Cracks faster than the shear wave speed. Science 284, 1337–1340.

Samudrala, O., Huang, Y., Rosakis, A.J., 2002. Subsonic and intersonic shear rupture of weak planes with a velocity weakening cohesive zone. J. Geophys. Res. 107 (B8), 2170.

Shi, Z.Q., Ben-Zion, Y., 2006. Dynamic rupture on a bi-material interface governed by slip-weakening friction. Geophys. J. Int. 165, 469–484.

Shi, Z.Q., Ben-Zion, Y., Needleman, A., 2007. Property of dynamic rupture and energy partition in a solid with a frictional interface. J. Mech. Phys. Solids doi:10.1016/j.jmps.2007.04.006, in press.

Spudich, P., Cranswick, E., 1984. Direct observation of rupture propagation during the 1979 Imperial Valley earthquake using a short baseline accelerometer array. Bull. Seismol. Soc. Am. 74 (6), 2083–2114.

Templeton, E.L., Rice, J.R., 2006. Extent and distribution of off-fault plasticity during seismic rupture including bimaterial effects. Eos Trans. AGU 87 (52) (Fall Meet. Suppl.) Abstract S34A-01.

Uenishi, K., Rice, J.R., 2003. Universal nucleation length for slip-weakening rupture instability under nonuniform fault loading. J. Geophys. Res. 108 (B1), 2042.

Xia, K., Rosakis, A.J., Kanamori, H., 2004. Laboratory earthquakes: the sub-Rayleigh-to-supershear rupture transition. Science 303, 1859–1861.

Xia, K., Rosakis, A.J., Kanamori, H., Rice, J.R., 2005. Laboratory earthquakes along inhomogeneous faults: directionality and supershear. Science 308, 681–684.

Zheng, G., Rice, J.R., 1998. Conditions under which velocity-weakening friction allows a self-healing versus a crack-like mode of rupture. Bull. Seismol. Soc. Am. 88, 1466–1483.